

Scalable Optimal Transport in High Dimensions for Graph Distances, Embedding Alignment, and More

Johannes Klicpera¹ Marten Lienen¹ Stephan Günnemann¹

Abstract

The current best practice for computing optimal transport (OT) is via entropy regularization and Sinkhorn iterations. This algorithm runs in quadratic time as it requires the full pairwise cost matrix, which is prohibitively expensive for large sets of objects. In this work we propose two effective log-linear time approximations of the cost matrix: First, a sparse approximation based on locality-sensitive hashing (LSH) and, second, a Nyström approximation with LSH-based sparse corrections, which we call locally corrected Nyström (LCN). These approximations enable general log-linear time algorithms for entropy-regularized OT that perform well even for the complex, high-dimensional spaces common in deep learning. We analyse these approximations theoretically and evaluate them experimentally both directly and end-to-end as a component for real-world applications. Using our approximations for unsupervised word embedding alignment enables us to speed up a state-of-the-art method by a factor of 3 while also improving the accuracy by 3.1 percentage points without any additional model changes. For graph distance regression we propose the graph transport network (GTN), which combines graph neural networks (GNNs) with enhanced Sinkhorn. GTN outcompetes previous models by 48 % and still scales log-linearly in the number of nodes.

1. Introduction

Measuring the distance between two distributions or sets of objects is a central problem in machine learning. One common method of solving this is optimal transport (OT). OT is concerned with the problem of finding the transport plan for moving a source distribution (e.g. a pile of earth) to

a sink distribution (e.g. a construction pit) with the cheapest cost w.r.t. some pointwise cost function (e.g. the Euclidean distance). The advantages of this method have been shown numerous times, e.g. in generative modelling (Arjovsky et al., 2017; Bousquet et al., 2017; Genevay et al., 2018), loss functions (Frogner et al., 2015), set matching (Wang et al., 2019), or domain adaptation (Courty et al., 2017). Motivated by this, many different methods for accelerating OT have been proposed in recent years (Indyk & Thaper, 2003; Papadakis et al., 2014; Backurs et al., 2020). However, most of these approaches are specialized methods that do not generalize to modern deep learning models, which rely on dynamically changing high-dimensional embeddings.

In this work we make OT computation for high-dimensional point sets more scalable by introducing two fast and accurate approximations of entropy-regularized optimal transport: Sparse Sinkhorn and LCN-Sinkhorn, the latter relying on our novel locally corrected Nyström (LCN) method. Sparse Sinkhorn uses a sparse cost matrix to leverage the fact that in entropy-regularized OT (also known as the Sinkhorn distance) (Cuturi, 2013) often only each point’s nearest neighbors influence the result. LCN-Sinkhorn extends this approach by leveraging LCN, a general similarity matrix approximation that fuses local (sparse) and global (low-rank) approximations, allowing us to simultaneously capture interactions between both close and far points. LCN-Sinkhorn thus fuses sparse Sinkhorn and Nyström-Sinkhorn (Altschuler et al., 2019). Both sparse Sinkhorn and LCN-Sinkhorn run in log-linear time.

We theoretically analyze these approximations and show that sparse corrections can lead to significant improvements over the Nyström approximation. We furthermore validate these approximations by showing that they are able to reproduce both the Sinkhorn distance and transport plan significantly better than previous methods across a wide range of regularization parameters and computational budgets (as e.g. demonstrated in Fig. 1). We then show the impact of these improvements by employing Sinkhorn approximations end-to-end in two high-impact machine learning tasks. First, we incorporate them into Wasserstein Procrustes for word embedding alignment (Grave et al., 2019). Without any further model changes LCN-Sinkhorn improves upon the

¹Technical University of Munich, Germany. Correspondence to: Johannes Klicpera <klicpera@in.tum.de>.

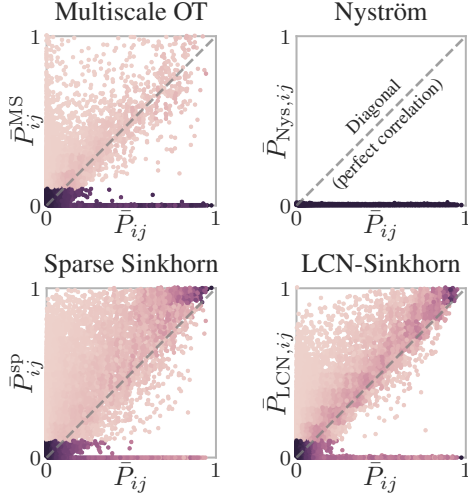


Figure 1: The proposed methods (sparse and LCN-Sinkhorn) show a clear correlation with the full Sinkhorn transport plan, as opposed to previous methods. Entries of approximations (y-axis) and full Sinkhorn (x-axis) for pre-aligned word embeddings (EN-DE). Color denotes density.

original method’s accuracy by 3.1 percentage points using a third of the training time. Second, we develop the graph transport network (GTN), which combines graph neural networks (GNNs) with optimal transport for graph distance regression, and further improve it via learnable unbalanced OT and multi-head OT. GTN with LCN-Sinkhorn is the first model that both overcomes the bottleneck of using a single embedding per graph and scales log-linearly in the number of nodes. Our implementation is available online.¹ In summary, our paper’s main contributions are:

- **Locally Corrected Nyström (LCN)**, a flexible log-linear time approximation for similarity matrices, merging local (sparse) and global (low-rank) approximations.
- Entropy-regularized optimal transport (a.k.a. Sinkhorn distance) with log-linear runtime via **sparse Sinkhorn** and **LCN-Sinkhorn**. These are the first log-linear approximations that are stable enough to substitute full entropy-regularized OT in models using high-dimensional spaces.
- The **graph transport network (GTN)**, a siamese GNN using multi-head unbalanced LCN-Sinkhorn. GTN both sets the state of the art on graph distance regression and still scales log-linearly in the number of nodes.

2. Entropy-regularized optimal transport

This work focuses on optimal transport between two discrete sets of points. We use entropy regularization, which enables fast computation and often performs better than regular OT

(Cuturi, 2013). Formally, given two categorical distributions modelled via the vectors $\mathbf{p} \in \mathbb{R}^n$ and $\mathbf{q} \in \mathbb{R}^m$ supported on two sets of points $X_p = \{\mathbf{x}_{p1}, \dots, \mathbf{x}_{pn}\}$ and $X_q = \{\mathbf{x}_{q1}, \dots, \mathbf{x}_{qm}\}$ in \mathbb{R}^d and the cost function $c : \mathbb{R}^d \times \mathbb{R}^d \rightarrow \mathbb{R}$ (e.g. the L_2 distance) giving rise to the cost matrix $\mathbf{C}_{ij} = c(\mathbf{x}_{pi}, \mathbf{x}_{qi})$ we aim to find the Sinkhorn distance d_c^λ and the associated optimal transport plan $\bar{\mathbf{P}}$ (Cuturi, 2013)

$$\begin{aligned} \bar{\mathbf{P}} &= \arg \min_{\mathbf{P}} \langle \mathbf{P}, \mathbf{C} \rangle_F - \lambda H(\mathbf{P}), \\ d_c^\lambda &= \langle \bar{\mathbf{P}}, \mathbf{C} \rangle_F - \lambda H(\bar{\mathbf{P}}), \\ \text{s.t. } \mathbf{P} \mathbf{1}_m &= \mathbf{p}, \mathbf{P}^T \mathbf{1}_n = \mathbf{q}, \end{aligned} \quad (1)$$

with the Frobenius inner product $\langle \cdot, \cdot \rangle_F$ and the entropy $H(\mathbf{P}) = -\sum_{i=1}^n \sum_{j=1}^m \mathbf{P}_{ij} \log \mathbf{P}_{ij}$. Note that d_c^λ includes the entropy and can thus be negative, while Cuturi (2013) originally used $d_{\text{Cuturi},c}^{1/\lambda} = \langle \bar{\mathbf{P}}, \mathbf{C} \rangle_F$. This optimization problem can be solved by finding the vectors $\bar{\mathbf{s}}$ and $\bar{\mathbf{t}}$ that normalize the columns and rows of the matrix $\bar{\mathbf{P}} = \text{diag}(\bar{\mathbf{s}}) \mathbf{K} \text{diag}(\bar{\mathbf{t}})$ with the similarity matrix $\mathbf{K}_{ij} = e^{-\frac{c_{ij}}{\lambda}}$, so that $\bar{\mathbf{P}} \mathbf{1}_m = \mathbf{p}$ and $\bar{\mathbf{P}}^T \mathbf{1}_n = \mathbf{q}$. We can achieve this via the Sinkhorn algorithm, which initializes the normalization vectors as $\mathbf{s}^{(1)} = \mathbf{1}_n$ and $\mathbf{t}^{(1)} = \mathbf{1}_m$ and updates them alternatingly via (Sinkhorn & Knopp, 1967)

$$\mathbf{s}^{(i)} = \mathbf{p} \oslash (\mathbf{K} \mathbf{t}^{(i-1)}), \quad \mathbf{t}^{(i)} = \mathbf{q} \oslash (\mathbf{K}^T \mathbf{s}^{(i)}) \quad (2)$$

until convergence, where \oslash denotes elementwise division.

3. Sparse Sinkhorn

The Sinkhorn algorithm is faster than non-regularized EMD algorithms, which run in $\mathcal{O}(n^2 m \log n \log(n \max(\mathbf{C})))$ (Tarjan, 1997). However, its computational cost is still quadratic in time $\mathcal{O}(nm)$, which is prohibitively expensive for large n and m . We overcome this by observing that the matrix \mathbf{K} , and hence also $\bar{\mathbf{P}}$, is negligibly small everywhere except at each point’s closest neighbors because of the exponential used in \mathbf{K} ’s computation. We propose to leverage this by approximating \mathbf{C} via the sparse matrix \mathbf{C}^{sp} , where

$$\mathbf{C}_{ij}^{\text{sp}} = \begin{cases} \mathbf{C}_{ij} & \text{if } \mathbf{x}_{pi} \text{ and } \mathbf{x}_{qj} \text{ are “near”,} \\ \infty & \text{otherwise.} \end{cases} \quad (3)$$

\mathbf{K}^{sp} and $\bar{\mathbf{P}}^{\text{sp}}$ follow from the definitions of \mathbf{K} and $\bar{\mathbf{P}}$. Finding “near” neighbors can be approximately solved via locality-sensitive hashing (LSH) on $X_p \cup X_q$.

Locality-sensitive hashing. LSH tries to filter “near” from “far” data points by putting them into different hash buckets. Points closer than a certain distance r_1 are put into the same bucket with probability at least p_1 , while those beyond some distance $r_2 = c \cdot r_1$ with $c > 1$ are put into the same bucket with probability at most $p_2 \ll p_1$. There is a plethora of LSH methods for different metric spaces and their associated cost (similarity/distance) functions (Wang et al., 2014;

¹<https://www.daml.in.tum.de/lcn>

Shrivastava & Li, 2014), and we can use any of them. In this work we focus on cross-polytope LSH (Andoni et al., 2015) and k -means LSH (Paulevé et al., 2010) (see App. H). We can control the (average) number of neighbors via the number of hash buckets. This allows sparse Sinkhorn with LSH to scale log-linearly with the number of points, i.e. $\mathcal{O}(n \log n)$ for $n \approx m$ (see App. A and App. K). Unfortunately, Sinkhorn with LSH can fail when e.g. the cost is evenly distributed or the matrix \mathbf{K}^{sp} does not have support (see App. B). However, we can alleviate these limitations by fusing \mathbf{K}^{sp} with the Nyström method.

4. Locally corrected Nyström and LCN-Sinkhorn

Nyström method. The Nyström method is a popular way of approximating similarity matrices that provides performance guarantees for many important tasks (Williams & Seeger, 2001; Musco & Musco, 2017). It approximates a positive semi-definite (PSD) similarity matrix \mathbf{K} via its low-rank decomposition $\mathbf{K}_{\text{Nys}} = \mathbf{U}\mathbf{A}^{-1}\mathbf{V}$. Since the optimal decomposition via SVD is too expensive to compute, Nyström instead chooses a set of l landmarks $L = \{\mathbf{x}_{l1}, \dots, \mathbf{x}_{ll}\}$ and obtains the matrices via $\mathbf{U}_{ij} = k(\mathbf{x}_{pi}, \mathbf{x}_{lj})$, $\mathbf{A}_{ij} = k(\mathbf{x}_{li}, \mathbf{x}_{lj})$, and $\mathbf{V}_{ij} = k(\mathbf{x}_{li}, \mathbf{x}_{qj})$, where $k(\mathbf{x}_1, \mathbf{x}_2)$ is an arbitrary PSD kernel, e.g. $k(\mathbf{x}_1, \mathbf{x}_2) = e^{-\frac{c(\mathbf{x}_1, \mathbf{x}_2)}{\lambda}}$ for Sinkhorn. Common methods of choosing landmarks from $X_p \cup X_q$ are uniform and ridge leverage score (RLS) sampling. We instead focus on k -means Nyström and sampling via k -means++, which we found to be significantly faster than recursive RLS sampling (Zhang et al., 2008) and perform better than both uniform and RLS sampling (see App. H).

Sparse vs. Nyström. Exponential kernels like the one used for \mathbf{K} (e.g. the Gaussian kernel) typically correspond to a reproducing kernel Hilbert space that is infinitely dimensional. The resulting Gram matrix \mathbf{K} thus usually has full rank. A low-rank approximation like the Nyström method can therefore only account for its global structure and not the local structure around each point \mathbf{x} . As such, it is ill-suited for any moderately low entropy regularization parameter, where the transport matrix $\bar{\mathbf{P}}$ resembles a permutation matrix. Sparse Sinkhorn, on the other hand, cannot account for global structure and instead approximates all non-selected distances as infinity. It will hence fail if more than a handful of neighbors are required per point. These approximations are thus opposites of each other, and as such not competing but rather *complementary* approaches.

Locally corrected Nyström. Since the entries in our sparse approximation are exact, we can directly fuse it with the Nyström approximation. For the indices of all non-zero values in the sparse approximation \mathbf{K}^{sp} we calculate the cor-

responding entries in the Nyström approximation, obtaining the sparse matrix $\mathbf{K}_{\text{Nys}}^{\text{sp}}$. To obtain the locally corrected Nyström (LCN) approximation² we subtract these entries from \mathbf{K}_{Nys} and replace them with their exact values, i.e.

$$\mathbf{K}_{\text{LCN}} = \mathbf{K}_{\text{Nys}} - \mathbf{K}_{\text{Nys}}^{\text{sp}} + \mathbf{K}^{\text{sp}} = \mathbf{K}_{\text{Nys}} + \mathbf{K}_{\Delta}^{\text{sp}}. \quad (4)$$

LCN-Sinkhorn. To obtain the approximate transport plan $\bar{\mathbf{P}}_{\text{LCN}}$ we run the Sinkhorn algorithm with \mathbf{K}_{LCN} instead of \mathbf{K} . However, we never fully instantiate \mathbf{K}_{LCN} . Instead, we directly use the decomposition and calculate the matrix-vector product in Eq. (2) as $\mathbf{K}_{\text{LCN}}\mathbf{t} = \mathbf{U}(\mathbf{A}^{-1}\mathbf{V}\mathbf{t}) + \mathbf{K}_{\Delta}^{\text{sp}}\mathbf{t}$, similarly to Altschuler et al. (2019). As a result we obtain the decomposed approximate OT plan $\bar{\mathbf{P}}_{\text{LCN}} = \bar{\mathbf{P}}_{\text{Nys}} + \bar{\mathbf{P}}_{\Delta}^{\text{sp}} = \bar{\mathbf{P}}_U \bar{\mathbf{P}}_W + \bar{\mathbf{P}}^{\text{sp}} - \bar{\mathbf{P}}_{\text{Nys}}^{\text{sp}}$ and the approximate distance (using Lemma A from Altschuler et al. (2019))

$$d_{\text{LCN},c}^{\lambda} = \lambda(s^T \bar{\mathbf{P}}_U \bar{\mathbf{P}}_W \mathbf{1}_m + \mathbf{1}_n^T \bar{\mathbf{P}}_U \bar{\mathbf{P}}_W \mathbf{t} + s^T \bar{\mathbf{P}}_{\Delta}^{\text{sp}} \mathbf{1}_m + \mathbf{1}_n^T \bar{\mathbf{P}}_{\Delta}^{\text{sp}} \mathbf{t}). \quad (5)$$

This approximation scales log-linearly with dataset size (see App. A and App. K for details). It allows us to smoothly move from Nyström-Sinkhorn to sparse Sinkhorn by varying the number of landmarks and neighbors. We can thus freely choose the optimal “operating point” based on the underlying problem and regularization parameter. We discuss the limitations of LCN-Sinkhorn in App. B.

5. Theoretical analysis

Approximation error. The main question we aim to answer in our theoretical analysis is what improvements to expect from adding sparse corrections to Nyström Sinkhorn. To do so, we first analyse approximations of \mathbf{K} in a uniform and a clustered data model. In these we use Nyström and LSH schemes that largely resemble k -means, as used in most of our experiments. Relevant proofs and notes for this section can be found in App. C to G.

Theorem 1. *Let X_p and X_q have n samples that are uniformly distributed on a d -dimensional closed, locally Euclidean manifold. Let $\mathbf{C}_{ij} = \|\mathbf{x}_{pi} - \mathbf{x}_{qj}\|_2$ and $\mathbf{K}_{ij} = e^{-\mathbf{C}_{ij}/\lambda}$. Let the landmarks be arranged a priori, with a minimum distance $2R$ between each other. Then the expected error of the Nyström approximation \mathbf{K}_{Nys} between a point \mathbf{x}_{pi} and its k th-nearest neighbor \mathbf{x}_{qi_k} is*

$$\mathbb{E}[\mathbf{K}_{i,i_k} - \mathbf{K}_{\text{Nys},i,i_k}] = \mathbb{E}[e^{-\delta_k/\lambda}] - \mathbb{E}[\mathbf{K}_{\text{Nys},i,i_k}], \quad (6)$$

with δ_k denoting the k th-nearest neighbor distance. With $\Gamma(\cdot, \cdot)$ denoting the upper incomplete Gamma function the

²LCN has an unrelated namesake on integrals, which uses high-order term to correct quadrature methods around singularities (Canino et al., 1998).

second term is bounded by

$$\mathbb{E}[\mathbf{K}_{\text{Nys},i,i_k}] \leq \frac{d(\Gamma(d) - \Gamma(d, 2R/\lambda))}{(2R/\lambda)^d} + \mathcal{O}(e^{-2R/\lambda}). \quad (7)$$

Eq. (6) is therefore dominated by $\mathbb{E}[e^{-\delta_k/\lambda}]$ if $\delta_k \ll R$, which is a reasonable assumption given that R only decreases slowly with the number of landmarks l since $R \geq ((d/2)!)^{1/d} \frac{1}{2\sqrt{\pi}}$ (Cohn, 2017). In this case the approximation's largest error is the one associated with the point's nearest neighbor. LCN uses the exact result for these nearest neighbors and therefore removes the largest errors, providing significant benefits even for uniform data. For example, just removing the first neighbor's error we obtain a 68 % decrease in the dominant first term ($d=32$, $\lambda=0.05$, $n=1000$). This is even more pronounced in clustered data.

Theorem 2. Let $X_p, X_q \subseteq \mathbb{R}^d$ be inside c (shared) clusters. Let r be the maximum L_2 distance of a point to its cluster center and D the minimum distance between different cluster centers, with $r \ll D$. Let $\mathbf{C}_{ij} = \|\mathbf{x}_{pi} - \mathbf{x}_{qj}\|_2$ and $\mathbf{K}_{ij} = e^{-\mathbf{C}_{ij}/\lambda}$. Let each LSH bucket used for the sparse approximation \mathbf{K}^{sp} cover at least one cluster. Let \mathbf{K}_{Nys} and \mathbf{K}_{LCN} both use one landmark at each cluster center. Then the maximum possible error is

$$\max_{\mathbf{x}_{pi}, \mathbf{x}_{qj}} \mathbf{K}_{ij} - \mathbf{K}_{\text{Nys},i,j} = 1 - e^{-2r/\lambda} - \mathcal{O}(e^{-2(D-r)/\lambda}), \quad (8)$$

$$\max_{\mathbf{x}_{pi}, \mathbf{x}_{qj}} \mathbf{K}_{ij} - \mathbf{K}_{ij}^{\text{sp}} = e^{-(D-2r)/\lambda}, \quad (9)$$

$$\max_{\mathbf{x}_{pi}, \mathbf{x}_{qj}} \mathbf{K}_{ij} - \mathbf{K}_{\text{LCN},i,j} = e^{-(D-2r)/\lambda} (1 - e^{-2r/\lambda} (2 - e^{-2r/\lambda}) + \mathcal{O}(e^{-2D/\lambda})). \quad (10)$$

This shows that the error in \mathbf{K}_{Nys} is close to 1 for any reasonably large $\frac{r}{\lambda}$ (which is the maximum error possible). The errors in \mathbf{K}^{sp} and \mathbf{K}_{LCN} on the other hand are vanishingly small in this case, since $r \ll D$.

The reduced maximum error directly translates to an improved Sinkhorn approximation. We can show this by adapting the Sinkhorn approximation error bounds due to Altschuler et al. (2019).

Definition 1. A generalized diagonal is the set of elements $M_{i\sigma(i)} \forall i \in \{1, \dots, n\}$ with matrix $\mathbf{M} \in \mathbb{R}^{n \times n}$ and permutation σ . A non-negative matrix has support if it has a strictly positive generalized diagonal. It has total support if $\mathbf{M} \neq 0$ and all non-zero elements lie on a strictly positive generalized diagonal.

Theorem 3. Let $X_p, X_q \subseteq \mathbb{R}^d$ have n samples. Denote ρ as the maximum distance between two samples. Let

$\tilde{\mathbf{K}}$ be a non-negative matrix with support, which approximates the similarity matrix \mathbf{K} with $\mathbf{K}_{ij} = e^{-\|\mathbf{x}_{pi} - \mathbf{x}_{qj}\|_2/\lambda}$ and $\max_{i,j} |\tilde{\mathbf{K}}_{ij} - \mathbf{K}_{ij}| \leq \frac{\epsilon'}{2} e^{-\rho/\lambda}$, where $\epsilon' = \min(1, \frac{\epsilon}{50(\rho+\lambda \log \frac{\lambda n}{\epsilon})})$. When performing the Sinkhorn algorithm until $\|\tilde{\mathbf{P}}\mathbf{1}_N - \mathbf{p}\|_1 + \|\tilde{\mathbf{P}}^T\mathbf{1}_N - \mathbf{q}\|_1 \leq \epsilon'/2$, the resulting approximate transport plan $\tilde{\mathbf{P}}$ and distance \tilde{d}_c^λ are bounded by

$$|d_c^\lambda - \tilde{d}_c^\lambda| \leq \epsilon, \quad D_{\text{KL}}(\tilde{\mathbf{P}} \| \tilde{\mathbf{P}}) \leq \epsilon/\lambda. \quad (11)$$

Convergence rate. We next show that sparse and LCN-Sinkhorn converge as fast as regular Sinkhorn by adapting the convergence bound by Dvurechensky et al. (2018) to account for sparsity.

Theorem 4. Given a non-negative matrix $\tilde{\mathbf{K}} \in \mathbb{R}^{n \times n}$ with support and $\mathbf{p} \in \mathbb{R}^n$, $\mathbf{q} \in \mathbb{R}^n$. The Sinkhorn algorithm gives a transport plan satisfying $\|\tilde{\mathbf{P}}\mathbf{1}_N - \mathbf{p}\|_1 + \|\tilde{\mathbf{P}}^T\mathbf{1}_N - \mathbf{q}\|_1 \leq \epsilon$ in iterations

$$k \leq 2 + \frac{-4 \ln(\min_{i,j} \{\tilde{\mathbf{K}}_{ij} | \tilde{\mathbf{K}}_{ij} > 0\} \min_{i,j} \{\mathbf{p}_i, \mathbf{q}_j\})}{\epsilon}. \quad (12)$$

Backpropagation. Efficient gradient computation is almost as important for modern deep learning models as the algorithm itself. These models usually aim at learning the embeddings in X_p and X_q and therefore need gradients w.r.t. the cost matrix \mathbf{C} . We can estimate these either via automatic differentiation of the unrolled Sinkhorn iterations or via the analytic solution that assumes exact convergence. Depending on the problem at hand, either the automatic or the analytic estimator will lead to faster overall convergence (Ablin et al., 2020). LCN-Sinkhorn works flawlessly with automatic backpropagation since it only relies on basic linear algebra (except for choosing Nyström landmarks and LSH neighbors, for which we use a simple straight-through estimator (Bengio et al., 2013)). To enable fast analytic backpropagation we provide analytic gradients in Proposition 1. Note that both backpropagation methods have runtime linear in the number of points n and m .

Proposition 1. In entropy-regularized OT and LCN-Sinkhorn the derivatives of the distances d_c^λ and $d_{\text{LCN},c}^\lambda$ (Eqs. (1) and (5)) and the optimal transport plan $\tilde{\mathbf{P}} \in \mathbb{R}^{n \times m}$ w.r.t. the (decomposed) cost matrix $\mathbf{C} \in \mathbb{R}^{n \times m}$ with total support are

$$\begin{aligned} \frac{\partial d_c^\lambda}{\partial \mathbf{C}} &= \tilde{\mathbf{P}}, \\ \frac{\partial d_{\text{LCN},c}^\lambda}{\partial \mathbf{U}} &= -\lambda \bar{\mathbf{s}} (\mathbf{W} \bar{\mathbf{t}})^T, \quad \frac{\partial d_{\text{LCN},c}^\lambda}{\partial \mathbf{W}} = -\lambda (\bar{\mathbf{s}}^T \mathbf{U})^T \bar{\mathbf{t}}^T, \\ \frac{\partial d_{\text{LCN},c}^\lambda}{\partial \log \mathbf{K}^{\text{sp}}} &= -\lambda \tilde{\mathbf{P}}^{\text{sp}}, \quad \frac{\partial d_{\text{LCN},c}^\lambda}{\partial \log \mathbf{K}_{\text{Nys}}^{\text{sp}}} = -\lambda \tilde{\mathbf{P}}_{\text{Nys}}^{\text{sp}}. \end{aligned} \quad (14)$$

This allows backpropagation in time $\mathcal{O}((n+m)l^2)$.

6. Graph transport network

Graph distance learning. Predicting similarities or distances between graph-structured objects is useful across a wide range of applications. It can be used to predict the reaction rate between molecules (Houston et al., 2019), or search for similar images (Johnson et al., 2015), similar molecules for drug discovery (Birchall et al., 2006), or similar code for vulnerability detection (Li et al., 2019). We propose the graph transport network (GTN) to evaluate approximate Sinkhorn on a full deep learning model and advance the state of the art on this task.

Graph transport network. GTN uses a Siamese graph neural network (GNN) to embed two graphs independently as *sets* of node embeddings. These sets are then matched using multi-head unbalanced OT. Node embeddings represent the nodes’ local environments, so similar neighborhoods will be close in embedding space and matched accordingly. Since Sinkhorn is symmetric and permutation invariant, any identical pair of graphs will thus by construction have a predicted distance of 0 (ignoring the entropy offset). More precisely, given an undirected graph $\mathcal{G} = (\mathcal{V}, \mathcal{E})$, with node set \mathcal{V} and edge set \mathcal{E} , node attributes $\mathbf{x}_i \in \mathbb{R}^{H_x}$ and (optional) edge attributes $\mathbf{e}_{i,j} \in \mathbb{R}^{H_e}$, with $i, j \in \mathcal{V}$, we update the node embeddings in each GNN layer via

$$\mathbf{h}_{\text{self},i}^{(l)} = \sigma(\mathbf{W}_{\text{node}}^{(l)} \mathbf{h}_i^{(l-1)} + \mathbf{b}^{(l)}), \quad (15)$$

$$\mathbf{h}_i^{(l)} = \mathbf{h}_{\text{self},i}^{(l)} + \sum_{j \in \mathcal{N}_i} \eta_{i,j}^{(l)} \mathbf{h}_{\text{self},j}^{(l)} \mathbf{W}_{\text{edge}} \mathbf{e}_{i,j}, \quad (16)$$

with \mathcal{N}_i denoting the neighborhood of node i , $\mathbf{h}_i^{(0)} = \mathbf{x}_i$, $\mathbf{h}_i^{(l)} \in \mathbb{R}^{H_N}$ for $l \geq 1$, the bilinear layer $\mathbf{W}_{\text{edge}} \in \mathbb{R}^{H_N \times H_N \times H_e}$, and the degree normalization $\eta_{i,j}^{(1)} = 1$ and $\eta_{i,j}^{(l)} = 1/\sqrt{\deg_i \deg_j}$ for $l > 1$. This choice of $\eta_{i,j}$ allows our model to handle highly skewed degree distributions while still being able to represent node degrees. We found the choice of non-linearity σ not to be critical and chose a LeakyReLU. We do not use the bilinear layer $\mathbf{W}_{\text{edge}} \mathbf{e}_{i,j}$ if there are no edge attributes. We aggregate each layer’s node embeddings to obtain the overall embedding of node i

$$\mathbf{h}_i^{\text{GNN}} = [\mathbf{h}_{\text{self},i}^{(1)} \parallel \mathbf{h}_i^{(1)} \parallel \mathbf{h}_i^{(2)} \parallel \dots \parallel \mathbf{h}_i^{(L)}]. \quad (17)$$

We then compute the embeddings for matching via $\mathbf{h}_i^{\text{final}} = \text{MLP}(\mathbf{h}_i^{\text{GNN}})$. Having obtained the embedding sets H_1^{final} and H_2^{final} of both graphs we use the L_2 distance as a cost function for the Sinkhorn distance. Finally, we calculate the prediction from the Sinkhorn distance via $d = d_c^\lambda w_{\text{out}} + b_{\text{out}}$, with learnable w_{out} and b_{out} . GTN is trained end-to-end via backpropagation. For small graphs we use the full Sinkhorn distance and scale to large graphs with LCN-Sinkhorn. GTN is more expressive than models that aggregate node embeddings to a single fixed-size embedding but still scales

log-linearly in the number of nodes, as opposed to previous approaches which scale quadratically.

Learnable unbalanced OT. Since GTN regularly encounters graphs with disagreeing numbers of nodes it needs to be able to handle cases where $\|\mathbf{p}\|_1 \neq \|\mathbf{q}\|_1$ or where not all nodes in one graph have a corresponding node in the other, i.e. $\mathbf{P}\mathbf{1}_m < \mathbf{p}$ or $\mathbf{P}^T\mathbf{1}_n < \mathbf{q}$. Unbalanced OT allows handling both of these cases (Peyré & Cuturi, 2019), usually by swapping the strict balancing requirements with a uniform divergence loss term on \mathbf{p} and \mathbf{q} (Frogner et al., 2015; Chizat et al., 2018). However, this *uniformly* penalizes deviations from balanced OT and therefore cannot adaptively ignore parts of the distribution. We propose to improve on this by swapping the cost matrix \mathbf{C} with the bipartite matching (BP) matrix (Riesen & Bunke, 2009)

$$\mathbf{C}_{\text{BP}} = \begin{bmatrix} \mathbf{C} & \mathbf{C}^{(\mathbf{p},\varepsilon)} \\ \mathbf{C}^{(\varepsilon,\mathbf{q})} & \mathbf{C}^{(\varepsilon,\varepsilon)} \end{bmatrix}, \quad \mathbf{C}_{ij}^{(\mathbf{p},\varepsilon)} = \begin{cases} c_{i,\varepsilon} & i = j \\ \infty & i \neq j \end{cases},$$

$$\mathbf{C}_{ij}^{(\varepsilon,\mathbf{q})} = \begin{cases} c_{\varepsilon,j} & i = j \\ \infty & i \neq j \end{cases}, \quad \mathbf{C}_{ij}^{(\varepsilon,\varepsilon)} = 0, \quad (18)$$

and obtain the deletion cost $c_{i,\varepsilon}$ and $c_{\varepsilon,j}$ from the input sets X_p and X_q . Using the BP matrix only adds minor computational overhead since we just need to save the diagonals $\mathbf{c}_{p,\varepsilon}$ and $\mathbf{c}_{\varepsilon,q}$ of $\mathbf{C}_{p,\varepsilon}$ and $\mathbf{C}_{\varepsilon,q}$. We can then use \mathbf{C}_{BP} in the Sinkhorn algorithm (Eq. (2)) via

$$\mathbf{K}_{\text{BP}} \mathbf{t} = \begin{bmatrix} \mathbf{K} \hat{\mathbf{t}} + \mathbf{c}_{p,\varepsilon} \odot \check{\mathbf{t}} \\ \mathbf{c}_{\varepsilon,q} \odot \hat{\mathbf{t}} + \mathbf{1}_n^T \check{\mathbf{t}} \end{bmatrix}, \quad \mathbf{K}_{\text{BP}}^T \mathbf{s} = \begin{bmatrix} \mathbf{K}^T \hat{\mathbf{s}} + \mathbf{c}_{\varepsilon,q} \odot \check{\mathbf{s}} \\ \mathbf{c}_{p,\varepsilon} \odot \hat{\mathbf{s}} + \mathbf{1}_m^T \check{\mathbf{s}} \end{bmatrix}, \quad (19)$$

where $\hat{\mathbf{t}}$ denotes the upper and $\check{\mathbf{t}}$ the lower part of the vector \mathbf{t} . To calculate d_c^λ we can decompose the transport plan \mathbf{P}_{BP} in the same way as \mathbf{C}_{BP} , with a single scalar for $\mathbf{P}_{\varepsilon,\varepsilon}$. For GTN we obtain the deletion cost via $c_{i,\varepsilon} = \|\boldsymbol{\alpha} \odot \mathbf{x}_{pi}\|_2$, with a learnable vector $\boldsymbol{\alpha} \in \mathbb{R}^d$.

Multi-head OT. Inspired by attention models (Vaswani et al., 2017) and multiscale kernels (Bermanis et al., 2013) we further improve GTN by using multiple OT heads. Using K heads means that we calculate K separate sets of embeddings representing the same pair of objects by using separate linear layers, i.e. $\mathbf{h}_{k,i}^{\text{final}} = \mathbf{W}^{(k)} \mathbf{h}_i^{\text{GNN}}$ for head k . We then calculate OT in parallel for these sets using a series of regularization parameters $\lambda_k = 2^{k-K/2} \lambda$. This yields a set of distances $d_c^\lambda \in \mathbb{R}^K$. We obtain the final prediction via $d = \text{MLP}(d_c^\lambda)$. Both learnable unbalanced OT and multi-head OT might be of independent interest.

7. Related work

Hierarchical kernel approximation. These methods usually hierarchically decompose the kernel matrix into sepa-

rate blocks and use low-rank or core-diagonal approximations for each block (Si et al., 2017; Ding et al., 2017). This idea is similar in spirit to LCN, but LCN boils it down to its essence by using one purely global part and a fine-grained LSH method to obtain one exact and purely local part.

Log-linear optimal transport. For an overview of optimal transport and its foundations see Peyré & Cuturi (2019). On low-dimensional grids and surfaces OT can be solved using dynamical OT (Papadakis et al., 2014; Solomon et al., 2014), convolutions (Solomon et al., 2015), or embedding/hashing schemes (Indyk & Thaper, 2003; Andoni et al., 2008). In higher dimensions we can use tree-based algorithms (Backurs et al., 2020) or hashing schemes (Charikar, 2002), which are however limited to a previously fixed set of points X_p, X_q , on which only the distributions p and q change. Another approach are sliced Wasserstein distances (Rabin et al., 2011). However, they do not provide a transport plan, require the L_2 distance as a cost function, and are either unstable in convergence or prohibitively expensive for high dimensions ($\mathcal{O}(nd^3)$) (Meng et al., 2019). For high-dimensional sets that change dynamically (e.g. during training) one method of achieving log-linear runtime is a multiscale approximation of entropy-regularized OT (Schmitzer, 2019; Gerber & Maggioni, 2017). Tenetov et al. (2018) recently proposed using a low-rank approximation of the Sinkhorn similarity matrix obtained via a semidiscrete approximation of the Euclidean distance. Altschuler et al. (2019) improved upon this approach by using the Nyström method for the approximation. However, these approaches still struggle with high-dimensional real-world problems, as we will show in Sec. 8.

Accelerating Sinkhorn. Another line of work has been pursuing accelerating entropy-regularized OT without changing its computational complexity w.r.t. the number of points. Original Sinkhorn requires $\mathcal{O}(1/\varepsilon^2)$ iterations, but Dvurechensky et al. (2018) and Jambulapati et al. (2019) recently proposed algorithms that reduce the computational complexity to $\mathcal{O}(\min(n^{9/4}/\varepsilon, n^2/\varepsilon^2))$ and $\mathcal{O}(n^2/\varepsilon)$, respectively. Mensch & Peyré (2020) proposed an online Sinkhorn algorithm to significantly reduce its memory cost. Alaya et al. (2019) proposed reducing the size of the Sinkhorn problem by screening out neglectable components, which allows for approximation guarantees. Genevay et al. (2016) proposed using a stochastic optimization scheme instead of Sinkhorn iterations. Essid & Solomon (2018) and Blondel et al. (2018) proposed alternative regularizations to obtain OT problems with similar runtimes as the Sinkhorn algorithm. This work is largely orthogonal to ours.

Embedding alignment. For an overview of cross-lingual word embedding models see Ruder et al. (2019). Unsupervised word embedding alignment was proposed by Conneau et al. (2018), with subsequent advances by Alvarez-Melis &

Jaakkola (2018); Grave et al. (2019); Joulin et al. (2018).

Graph matching and distance learning. Graph neural networks (GNNs) have recently been successful on a wide variety of graph-based tasks (Kipf & Welling, 2017; Klicpera et al., 2019; 2020; Zambaldi et al., 2019). GNN-based approaches for graph matching and graph distance learning either rely on a single fixed-dimensional graph embedding (Bai et al., 2019; Li et al., 2019), or only use attention or some other strongly simplified variant of optimal transport (Bai et al., 2019; Riba et al., 2018; Li et al., 2019). Others break permutation invariance and are thus ill-suited for this task (Ktena et al., 2017; Bai et al., 2018). So far only approaches using a single graph embedding allow faster than quadratic scaling in the number of nodes. Compared to the Sinkhorn-based image model proposed by Wang et al. (2019) GTN uses no CNN or cross-graph attention, but an enhanced GNN and embedding aggregation scheme. OT has recently been proposed for graph kernels (Maretic et al., 2019; Vayer et al., 2019), which can (to some extent) be used for graph matching, but not for distance learning.

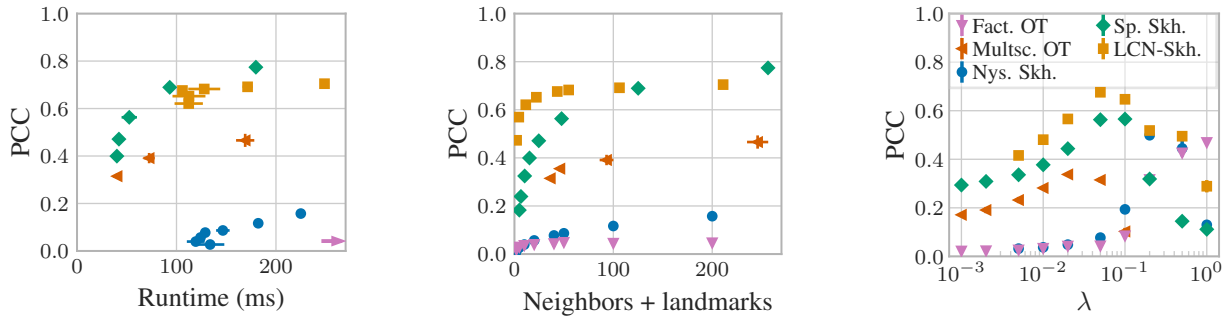
8. Experiments

Approximating Sinkhorn. We start by directly investigating different Sinkhorn approximations. To do so we compute entropy-regularized OT on (i) pairs of 10^4 word embeddings from Conneau et al. (2018), which we preprocess with Wasserstein Procrustes alignment in order to obtain both close and distant neighbors, (ii) the armadillo and dragon point clouds from the Stanford 3D Scanning Repository (Stanford, 2014) (with 10^4 randomly subsampled points), and (iii) pairs of 10^4 data points that are uniformly distributed in the d -ball ($d = 16$). We let every method use the same total number of 40 average neighbors and landmarks (LCN uses 20 each) and set $\lambda = 0.05$ (as e.g. in Grave et al. (2019)). Besides the Sinkhorn distance we measure transport plan approximation quality by (a) calculating the Pearson correlation coefficient (PCC) between all entries in the approximated plan and the true \bar{P} and (b) comparing the sets of 0.1 % largest entries in the approximated and true \bar{P} using the Jaccard similarity (intersection over union, IoU). Note that usually the OT plan is more important than the distance, since it determines the training gradient and tasks like embedding alignment are exclusively based on the OT plan. In all figures the error bars denote standard deviation across 5 runs, which is often too small to be visible.

Table 1 shows that for word embeddings both sparse Sinkhorn, LCN-Sinkhorn and factored OT (Forrow et al., 2019) obtain distances that are significantly closer to the true d_c^λ than Multiscale OT and Nyström-Sinkhorn. Furthermore, the transport plan computed by sparse Sinkhorn and LCN-Sinkhorn show both a PCC and IoU that are around twice as high as Multiscale OT, while Nyström-Sinkhorn and

Table 1: Mean and standard deviation of relative Sinkhorn distance error, IoU of top 0.1 % and correlation coefficient (PCC) of OT plan entries across 5 runs. Sparse Sinkhorn and LCN-Sinkhorn achieve the best approximation in all 3 measures.

	EN-DE			EN-ES			3D point cloud			Uniform in d -ball ($d=16$)		
	Rel. err. d_c^λ	PCC	IoU	Rel. err. d_c^λ	PCC	IoU	Rel. err. d_c^λ	PCC	IoU	Rel. err. d_c^λ	PCC	IoU
Factored OT	0.318 ± 0.001	0.044 ± 0.001	0.019 ± 0.002	0.332 ± 0.001	0.037 ± 0.002	0.026 ± 0.005	6.309 ± 0.004	0.352 ± 0.001	0.004 ± 0.001	1.796 ± 0.001	0.096 ± 0.001	0.029 ± 0.000
Multiscale OT	0.634 ± 0.011	0.308 ± 0.014	0.123 ± 0.005	0.645 ± 0.014	0.321 ± 0.006	0.125 ± 0.012	0.24 ± 0.07	0.427 ± 0.008	0.172 ± 0.011	0.03 ± 0.02	0.091 ± 0.005	0.021 ± 0.001
Nyström Skh.	1.183 ± 0.005	0.077 ± 0.001	0.045 ± 0.005	1.175 ± 0.018	0.068 ± 0.001	0.048 ± 0.006	1.89 ± 0.07	0.559 ± 0.009	0.126 ± 0.014	1.837 ± 0.006	0.073 ± 0.000	0.018 ± 0.000
Sparse Skh.	0.233 ± 0.002	0.552 ± 0.004	0.102 ± 0.001	0.217 ± 0.001	0.623 ± 0.004	0.102 ± 0.001	0.593 ± 0.015	0.44 ± 0.03	0.187 ± 0.014	0.241 ± 0.002	0.341 ± 0.004	0.090 ± 0.001
LCN-Sinkhorn	0.406 ± 0.015	0.673 ± 0.012	0.197 ± 0.007	0.368 ± 0.012	0.736 ± 0.003	0.201 ± 0.003	1.91 ± 0.28	0.564 ± 0.008	0.195 ± 0.013	0.435 ± 0.009	0.328 ± 0.006	0.079 ± 0.001


 Figure 2: OT plan approximation quality for EN-DE, via PCC. **Left:** Sparse Sinkhorn offers the best tradeoff with runtime, with LCN-Sinkhorn closely behind. **Center:** LCN-Sinkhorn achieves the best approximation for low and sparse Sinkhorn for high numbers of neighbors/landmarks. **Right:** Sparse Sinkhorn performs best for low, LCN-Sinkhorn for moderate and factored OT for very high entropy regularization λ . The arrow indicates factored OT results far outside the range.

factored OT exhibit almost no correlation. LCN-Sinkhorn performs especially well in this regard. This is also evident in Fig. 1, which shows how the $10^4 \times 10^4$ approximated OT plan entries compared to the true Sinkhorn values. Multiscale OT shows the best distance approximation on 3D point clouds and random high-dimensional data. However, sparse Sinkhorn and LCN-Sinkhorn remain the best OT plan approximations, especially in high dimensions.

Fig. 2 shows that sparse Sinkhorn offers the best trade-off between runtime and OT plan quality. Factored OT exhibits a runtime 2 to 10 times longer than the competition due to its iterative refinement scheme. LCN-Sinkhorn performs best for use cases with constrained memory (few neighbors/landmarks). The number of neighbors and landmarks directly determines memory usage and is linearly proportional to the runtime (see App. K). Fig. 2 furthermore shows that sparse Sinkhorn performs best for low regularizations, where LCN-Sinkhorn fails due to the Nyström part going out of bounds. Nyström Sinkhorn performs best at high values and LCN-Sinkhorn always performs better than both (as long as it can be calculated). Interestingly,

all approximations except factored OT seem to fail at high λ . We defer analogously discussing the distance approximation to App. L. All approximations scale linearly both in the number of neighbors/landmarks and dataset size, as shown in App. K. Overall, we see that sparse Sinkhorn and LCN-Sinkhorn yield significant improvements over previous approximations. However, do these improvements also translate to better performance on downstream tasks?

Embedding alignment. Embedding alignment is the task of finding the orthogonal matrix $R \in \mathbb{R}^{d \times d}$ that best aligns the vectors from two different embedding spaces, which is e.g. useful for unsupervised word translation. We use the experimental setup established by Conneau et al. (2018) by migrating Grave et al. (2019)’s implementation to PyTorch. The only change we make is using the full set of 20 000 word embeddings and training for 300 steps, while reducing the learning rate by half every 100 steps. We do not change *any* other hyperparameters and do not use unbalanced OT. After training we match pairs via cross-domain similarity local scaling (CSLS) (Conneau et al., 2018). We use 10 Sinkhorn iterations, 40 neighbors on average for sparse Sinkhorn, and

Table 2: Accuracy and standard deviation across 5 runs for unsupervised word embedding alignment with Wasserstein Procrustes. LCN-Sinkhorn improves upon the original by 3.1 pp. before and 2.0 pp. after iterative CSLS refinement. *Migrated and re-run on GPU via PyTorch

	Time (s)	EN-ES	ES-EN	EN-FR	FR-EN	EN-DE	DE-EN	EN-RU	RU-EN	Avg.
Original*	268	79.2 \pm 0.2	78.8 \pm 2.8	81.0 \pm 0.3	79.4 \pm 0.9	71.7 \pm 0.2	65.7 \pm 3.4	36.3 \pm 1.1	51.1 \pm 1.1	67.9
Full Sinkhorn	402	81.1 \pm 0.0	82.0 \pm 0.0	81.2 \pm 0.0	81.3 \pm 0.0	74.1 \pm 0.0	70.7 \pm 0.0	37.3 \pm 0.0	53.5 \pm 0.0	70.1
Multiscale OT	88.2	24 \pm 31	74.7 \pm 3.3	27 \pm 32	6.3 \pm 4.4	36 \pm 10	47 \pm 21	0.0 \pm 0.0	0.2 \pm 0.1	26.8
Nyström Skh.	102	64.4 \pm 1.0	59.3 \pm 1.2	64.1 \pm 1.6	56.8 \pm 4.0	54.1 \pm 0.6	47.1 \pm 3.5	14.1 \pm 1.2	22.5 \pm 2.4	47.8
Sparse Skh.	49.2	80.2 \pm 0.2	81.7 \pm 0.4	80.9 \pm 0.3	80.1 \pm 0.2	72.1 \pm 0.6	65.1 \pm 1.7	35.5 \pm 0.6	51.5 \pm 0.4	68.4
LCN-Sinkhorn	86.8	81.8 \pm 0.2	81.3 \pm 1.8	82.0 \pm 0.4	82.1 \pm 0.3	73.6 \pm 0.2	71.3 \pm 0.9	41.0 \pm 0.8	55.1 \pm 1.4	71.0
Original* + ref.	268+81	83.0 \pm 0.3	82.0 \pm 2.5	83.8 \pm 0.1	83.0 \pm 0.4	77.3 \pm 0.3	69.7 \pm 4.3	46.2 \pm 1.0	54.0 \pm 1.1	72.4
LCN-Skh. + ref.	86.8+81	83.5 \pm 0.2	83.1 \pm 1.3	83.8 \pm 0.2	83.6 \pm 0.1	77.2 \pm 0.3	72.8 \pm 0.7	51.8 \pm 2.6	59.2 \pm 1.9	74.4

20 neighbors and landmarks for LCN-Sinkhorn (for details see App. H). We allow both multiscale OT and Nyström Sinkhorn to use as many landmarks and neighbors as can fit into GPU memory and finetune both methods.

Table 2 shows that using full Sinkhorn yields a significant improvement in accuracy on this task compared to the original approach of performing Sinkhorn on randomly sampled subsets of embeddings (Grave et al., 2019). LCN-Sinkhorn even outperforms the *full* version in most cases, which is likely due to regularization effects from the approximation. It also runs 4.6x faster than full Sinkhorn and 3.1x faster than the original scheme, while using 88 % and 44 % less memory, respectively. Sparse Sinkhorn runs 1.8x faster than LCN-Sinkhorn but cannot match its accuracy. LCN-Sinkhorn still outcompetes the original method after refining the embeddings with iterative local CSLS (Conneau et al., 2018). Both multiscale OT and Nyström Sinkhorn fail at this task, despite their larger computational budget. This shows that the improvements achieved by sparse Sinkhorn and LCN-Sinkhorn have an even larger impact in practice.

Graph distance regression. The graph edit distance (GED) is useful for various tasks such as image retrieval (Xiao et al., 2008) or fingerprint matching (Neuhaus & Bunke, 2004), but its computation is NP-complete (Bunke & Shearer, 1998). For large graphs we therefore need an effective approximation. We use the Linux dataset by Bai et al. (2019) and generate 2 new datasets by computing the exact GED using the method by Lerouge et al. (2017) on small graphs (≤ 30 nodes) from the AIDS dataset (Riesen & Bunke, 2008) and a set of preferential attachment graphs. We compare GTN to 3 state-of-the-art baselines: SiameseMPNN (Riba et al., 2018), SimGNN (Bai et al., 2019), and the Graph Matching Network (GMN) (Li et al., 2019). We tune the hyperparameters of all baselines and GTN via grid search. For more details see App. H to J.

We first test GTN and the proposed OT enhancements. Table 3 shows that GTN improves upon other models by 20 % with a single head and by 48 % with 8 OT heads. Its per-

Table 3: RMSE for GED regression across 3 runs and the targets’ standard deviation σ . GTN outperforms previous models by 48 %.

	Linux	AIDS30	Pref. att.
σ	0.184	16.2	48.3
SiamMPNN	0.090 \pm 0.007	13.8 \pm 0.3	12.1 \pm 0.6
SimGNN	0.039	4.5 \pm 0.3	8.3 \pm 1.4
GMN	0.015 \pm 0.000	10.3 \pm 0.6	7.8 \pm 0.3
GTN, 1 head	0.022 \pm 0.001	3.7 \pm 0.1	4.5 \pm 0.3
8 OT heads	0.012 \pm 0.001	3.2 \pm 0.1	3.5 \pm 0.2
Unbalanced OT	0.033 \pm 0.002	15.7 \pm 0.5	9.7 \pm 0.9
Balanced OT	0.034 \pm 0.001	15.3 \pm 0.1	27.4 \pm 0.9

Table 4: RMSE for graph distance regression across 3 runs and the targets’ standard deviation σ . Using LCN-Sinkhorn with GTN increases the error by only 10 % and allows log-linear scaling.

	GED		PM [10^{-2}]
	AIDS30	Pref. att.	Pref. att. 200
σ	16.2	48.3	10.2
Full Sinkhorn	3.7 \pm 0.1	4.5 \pm 0.3	1.27 \pm 0.06
Nyström Skh.	3.6 \pm 0.3	6.2 \pm 0.6	2.43 \pm 0.07
Multiscale OT	11.2 \pm 0.3	27.4 \pm 5.4	6.71 \pm 0.44
Sparse Skh.	44 \pm 30	40.7 \pm 8.1	7.57 \pm 1.09
LCN-Skh.	4.0 \pm 0.1	5.1 \pm 0.4	1.41 \pm 0.15

formance breaks down with regular unbalanced (using KL-divergence loss for the marginals) and balanced OT, showing the importance of learnable unbalanced OT.

Having established GTN as a state-of-the-art model we next ask whether we can sustain its performance when using approximate OT. For this we additionally generate a set of larger graphs with around 200 nodes and use the Pyramid matching (PM) kernel (Nikolentzos et al., 2017) as the prediction target, since these graphs are too large to compute the GED. See App. J for hyperparameter details. Table 4 shows that both sparse Sinkhorn and the multiscale method using

4 (expected) neighbors fail at this task, demonstrating that the low-rank approximation in LCN has a crucial stabilizing effect during training. Nyström Sinkhorn with 4 landmarks performs surprisingly well on the AIDS30 dataset, suggesting an overall low-rank structure with Nyström acting as regularization. However, it does not perform as well on the other two datasets. Using LCN-Sinkhorn with 2 neighbors and landmarks works well on all three datasets, with an RMSE increased by only 10 % compared to full GTN. App. K furthermore shows that GTN with LCN-Sinkhorn indeed scales linearly in the number of nodes across multiple orders of magnitude. This model thus enables graph matching and distance learning on graphs that are considered large even for simple node-level tasks (20 000 nodes).

9. Conclusion

Locality-sensitive hashing (LSH) and the novel locally corrected Nyström (LCN) method enable fast and accurate approximations of entropy-regularized OT with log-linear runtime: Sparse Sinkhorn and LCN-Sinkhorn. The graph transport network (GTN) is one example for such a model, which can be substantially improved with learnable unbalanced OT and multi-head OT. It sets the new state of the art for graph distance learning while still scaling log-linearly with graph size. These contributions enable new applications and models that are both faster and more accurate, since they can sidestep workarounds such as pooling.

ACKNOWLEDGMENTS

We would like to thank Johannes Pitz, Oleksandr Shchur, Aleksandar Bojchevski, and Daniel Zügner for their support, suggestions, and feedback during the process of creating this paper. This research was supported by the Deutsche Forschungsgemeinschaft (DFG) through the Emmy Noether grant GU 1409/2-1 and the TUM International Graduate School of Science and Engineering (IGSSE), GSC 81.

References

- Pierre Ablin, Gabriel Peyré, and Thomas Moreau. Super-efficiency of automatic differentiation for functions defined as a minimum. In *ICML*, 2020.
- Mokhtar Z. Alaya, Maxime Berar, Gilles Gasso, and Alain Rakotomamonjy. Screening Sinkhorn Algorithm for Regularized Optimal Transport. In *NeurIPS*, 2019.
- Jason Altschuler, Francis Bach, Alessandro Rudi, and Jonathan Niles-Weed. Massively scalable Sinkhorn distances via the Nyström method. In *NeurIPS*, 2019.
- David Alvarez-Melis and Tommi S. Jaakkola. Gromov-Wasserstein Alignment of Word Embedding Spaces. In *EMNLP*, 2018.
- Alexandr Andoni, Piotr Indyk, and Robert Krauthgamer. Earth mover distance over high-dimensional spaces. In *ACM-SIAM symposium on Discrete algorithms (SODA)*, 2008.
- Alexandr Andoni, Piotr Indyk, Thijs Laarhoven, Ilya P. Razenshteyn, and Ludwig Schmidt. Practical and Optimal LSH for Angular Distance. In *NeurIPS*, 2015.
- Martin Arjovsky, Soumith Chintala, and Léon Bottou. Wasserstein Generative Adversarial Networks. In *ICML*, 2017.
- Arturs Backurs, Yihe Dong, Piotr Indyk, Ilya Razenshteyn, and Tal Wagner. Scalable Nearest Neighbor Search for Optimal Transport. In *ICML*, 2020.
- Yunsheng Bai, Hao Ding, Yizhou Sun, and Wei Wang. Convolutional Set Matching for Graph Similarity. In *Relational Representation Learning Workshop, NeurIPS*, 2018.
- Yunsheng Bai, Hao Ding, Song Bian, Ting Chen, Yizhou Sun, and Wei Wang. SimGNN: A Neural Network Approach to Fast Graph Similarity Computation. In *WSDM*, 2019.
- Yoshua Bengio, Nicholas Léonard, and Aaron Courville. Estimating or Propagating Gradients Through Stochastic Neurons for Conditional Computation. *arXiv*, 1308.3432, 2013.
- Christian Berg, Jens Peter Reus Christensen, and Paul Reszel. *Harmonic Analysis on Semigroups*. Number 100 in Graduate Texts in Mathematics. 1984.
- Amit Bermanis, Amir Averbuch, and Ronald R. Coifman. Multiscale data sampling and function extension. *Applied and Computational Harmonic Analysis*, 34(1):15–29, 2013.
- Kristian Birchall, Valerie J. Gillet, Gavin Harper, and Stephen D. Pickett. Training Similarity Measures for Specific Activities: Application to Reduced Graphs. *Journal of Chemical Information and Modeling*, 46(2):577–586, 2006.
- Mathieu Blondel, Vivien Seguy, and Antoine Rolet. Smooth and Sparse Optimal Transport. In *AISTATS*, 2018.
- Olivier Bousquet, Sylvain Gelly, Ilya Tolstikhin, Carl-Johann Simon-Gabriel, and Bernhard Schölkopf. From optimal transport to generative modeling: the VEGAN cookbook. *arXiv*, 1705.07642, 2017.
- Horst Bunke and Kim Shearer. A graph distance metric based on the maximal common subgraph. *Pattern Recognition Letters*, 19(3):255–259, 1998.

- Lawrence F. Canino, John J. Ottusch, Mark A. Stalzer, John L. Visser, and Stephen M. Wandzura. Numerical Solution of the Helmholtz Equation in 2D and 3D Using a High-Order Nyström Discretization. *Journal of Computational Physics*, 146(2):627–663, 1998.
- Moses Charikar. Similarity estimation techniques from rounding algorithms. In *ACM symposium on Theory of computing (STOC)*, 2002.
- Lénaïc Chizat, Gabriel Peyré, Bernhard Schmitzer, and François-Xavier Vialard. Scaling algorithms for unbalanced optimal transport problems. *Mathematics of Computation*, 87(314):2563–2609, 2018.
- Henry Cohn. A Conceptual Breakthrough in Sphere Packing. *Notices of the American Mathematical Society*, 64(02):102–115, 2017.
- Alexis Conneau, Guillaume Lample, Marc’Aurelio Ranzato, Ludovic Denoyer, and Hervé Jégou. Word translation without parallel data. In *ICLR*, 2018.
- Nicolas Courty, Rémi Flamary, Amaury Habrard, and Alain Rakotomamonjy. Joint distribution optimal transportation for domain adaptation. In *NeurIPS*, 2017.
- Marco Cuturi. Sinkhorn Distances: Lightspeed Computation of Optimal Transport. In *NeurIPS*, 2013.
- Yi Ding, Risi Kondor, and Jonathan Eskreis-Winkler. Multiresolution Kernel Approximation for Gaussian Process Regression. In *NeurIPS*, 2017.
- Pavel E. Dvurechensky, Alexander Gasnikov, and Alexey Kroshnin. Computational Optimal Transport: Complexity by Accelerated Gradient Descent Is Better Than by Sinkhorn’s Algorithm. In *ICML*, 2018.
- Montacer ESSID and Justin Solomon. Quadratically Regularized Optimal Transport on Graphs. *SIAM Journal on Scientific Computing*, 40(4):A1961–A1986, 2018.
- Matthias Fey and Jan E. Lenssen. Fast Graph Representation Learning with PyTorch Geometric. In *Workshop on Representation Learning on Graphs and Manifolds, ICLR*, 2019.
- Aden Forrow, Jan-Christian Hütter, Mor Nitzan, Philippe Rigollet, Geoffrey Schiebinger, and Jonathan Weed. Statistical Optimal Transport via Factored Couplings. In *AISTATS*, 2019.
- Charlie Frogner, Chiyuan Zhang, Hossein Mobahi, Mauricio Araya-Polo, and Tomaso A. Poggio. Learning with a Wasserstein Loss. In *NeurIPS*, 2015.
- Aude Genevay, Marco Cuturi, Gabriel Peyré, and Francis R. Bach. Stochastic Optimization for Large-scale Optimal Transport. In *NeurIPS*, 2016.
- Aude Genevay, Gabriel Peyré, and Marco Cuturi. Learning Generative Models with Sinkhorn Divergences. In *AISTATS*, 2018.
- Samuel Gerber and Mauro Maggioni. Multiscale Strategies for Computing Optimal Transport. *J. Mach. Learn. Res.*, 18:72:1–72:32, 2017.
- Edouard Grave, Armand Joulin, and Quentin Berthet. Unsupervised Alignment of Embeddings with Wasserstein Procrustes. In *AISTATS*, 2019.
- Paul L. Houston, Apurba Nandi, and Joel M. Bowman. A Machine Learning Approach for Prediction of Rate Constants. *The Journal of Physical Chemistry Letters*, 10(17):5250–5258, 2019.
- Piotr Indyk and Nitin Thaper. Fast image retrieval via embeddings. In *International Workshop on Statistical and Computational Theories of Vision, ICCV*, 2003.
- Arun Jambulapati, Aaron Sidford, and Kevin Tian. A Direct $\tilde{O}(1/\epsilon)$ Iteration Parallel Algorithm for Optimal Transport. In *NeurIPS*, 2019.
- Justin Johnson, Ranjay Krishna, Michael Stark, Li-Jia Li, David A. Shamma, Michael S. Bernstein, and Fei-Fei Li. Image retrieval using scene graphs. In *CVPR*, 2015.
- Armand Joulin, Piotr Bojanowski, Tomas Mikolov, Hervé Jégou, and Edouard Grave. Loss in Translation: Learning Bilingual Word Mapping with a Retrieval Criterion. In *EMNLP*, 2018.
- Thomas N. Kipf and Max Welling. Semi-Supervised Classification with Graph Convolutional Networks. In *ICLR*, 2017.
- Johannes Klicpera, Aleksandar Bojchevski, and Stephan Günnemann. Predict then Propagate: Graph Neural Networks Meet Personalized PageRank. In *ICLR*, 2019.
- Johannes Klicpera, Janek Groß, and Stephan Günnemann. Directional Message Passing for Molecular Graphs. In *ICLR*, 2020.
- Sofia Ira Ktena, Sarah Parisot, Enzo Ferrante, Martin Rajchl, Matthew Lee, Ben Glocker, and Daniel Rueckert. Distance Metric Learning Using Graph Convolutional Networks: Application to Functional Brain Networks. In *MICCAI*, 2017.
- Julien Lerouge, Zeina Abu-Aisheh, Romain Raveaux, Pierre Héroux, and Sébastien Adam. New binary linear programming formulation to compute the graph edit distance. *Pattern Recognit.*, 72:254–265, 2017.

- Yujia Li, Chenjie Gu, Thomas Dullien, Oriol Vinyals, and Pushmeet Kohli. Graph Matching Networks for Learning the Similarity of Graph Structured Objects. In *ICML*, 2019.
- Hermína Petric Maretic, Mireille El Gheche, Giovanni Chierchia, and Pascal Frossard. GOT: An Optimal Transport framework for Graph comparison. In *NeurIPS*, 2019.
- Cheng Meng, Yuan Ke, Jingyi Zhang, Mengrui Zhang, Wenxuan Zhong, and Ping Ma. Large-scale optimal transport map estimation using projection pursuit. In *NeurIPS*, 2019.
- Arthur Mensch and Gabriel Peyré. Online Sinkhorn: Optimal Transport distances from sample streams. In *NeurIPS*, 2020.
- Cameron Musco and Christopher Musco. Recursive Sampling for the Nystrom Method. In *NeurIPS*, 2017.
- Michel Neuhaus and Horst Bunke. An Error-Tolerant Approximate Matching Algorithm for Attributed Planar Graphs and Its Application to Fingerprint Classification. In *Structural, Syntactic, and Statistical Pattern Recognition*, 2004.
- Giannis Nikolentzos, Polykarpos Meladianos, and Michalis Vazirgiannis. Matching Node Embeddings for Graph Similarity. In *AAAI*, 2017.
- David Nistér and Henrik Stewénus. Scalable Recognition with a Vocabulary Tree. In *CVPR*, 2006.
- Nicolas Papadakis, Gabriel Peyré, and Édouard Oudet. Optimal Transport with Proximal Splitting. *SIAM J. Imaging Sciences*, 7(1):212–238, 2014.
- Adam Paszke, Sam Gross, Francisco Massa, Adam Lerer, James Bradbury, Gregory Chanan, Trevor Killeen, Zeming Lin, Natalia Gimelshein, Luca Antiga, Alban Desmaison, Andreas Köpf, Edward Yang, Zachary DeVito, Martin Raison, Alykhan Tejani, Sasank Chilamkurthy, Benoit Steiner, Lu Fang, Junjie Bai, and Soumith Chintala. PyTorch: An Imperative Style, High-Performance Deep Learning Library. In *NeurIPS*, 2019.
- Loïc Paulevé, Hervé Jégou, and Laurent Amsaleg. Locality sensitive hashing: A comparison of hash function types and querying mechanisms. *Pattern Recognit. Lett.*, 31(11):1348–1358, 2010.
- Allon G Percus and Olivier C Martin. Scaling Universalities of kth-Nearest Neighbor Distances on Closed Manifolds. *Advances in Applied Mathematics*, 21(3):424–436, 1998.
- Gabriel Peyré and Marco Cuturi. Computational Optimal Transport. *Foundations and Trends in Machine Learning*, 11(5-6):355–607, 2019.
- Julien Rabin, Gabriel Peyré, Julie Delon, and Marc Bernot. Wasserstein Barycenter and Its Application to Texture Mixing. In *Scale Space and Variational Methods in Computer Vision (SSVM)*, 2011.
- Pau Riba, Andreas Fischer, Josep Lladós, and Alicia Fornés. Learning Graph Distances with Message Passing Neural Networks. In *ICPR*, 2018.
- Kaspar Riesen and Horst Bunke. IAM Graph Database Repository for Graph Based Pattern Recognition and Machine Learning. In *Structural, Syntactic, and Statistical Pattern Recognition*, 2008.
- Kaspar Riesen and Horst Bunke. Approximate graph edit distance computation by means of bipartite graph matching. *Image Vis. Comput.*, 27(7):950–959, 2009.
- Sebastian Ruder, Ivan Vulic, and Anders Søgaard. A Survey of Cross-lingual Word Embedding Models. *J. Artif. Intell. Res.*, 65:569–631, 2019.
- Bernhard Schmitzer. Stabilized Sparse Scaling Algorithms for Entropy Regularized Transport Problems. *SIAM Journal on Scientific Computing*, 41(3):A1443–A1481, 2019.
- Anshumali Shrivastava and Ping Li. Asymmetric LSH (ALSH) for Sublinear Time Maximum Inner Product Search (MIPS). In *NeurIPS*, 2014.
- Si Si, Cho-Jui Hsieh, and Inderjit S. Dhillon. Memory Efficient Kernel Approximation. *Journal of Machine Learning Research*, 18(20):1–32, 2017.
- Richard Sinkhorn and Paul Knopp. Concerning nonnegative matrices and doubly stochastic matrices. *Pacific Journal of Mathematics*, 21(2):343–348, 1967.
- Justin Solomon, Raif M. Rustamov, Leonidas J. Guibas, and Adrian Butscher. Earth mover’s distances on discrete surfaces. *ACM Trans. Graph.*, 33(4):67:1–67:12, 2014.
- Justin Solomon, Fernando de Goes, Gabriel Peyré, Marco Cuturi, Adrian Butscher, Andy Nguyen, Tao Du, and Leonidas J. Guibas. Convolutional wasserstein distances: efficient optimal transportation on geometric domains. *ACM Trans. Graph.*, 34(4):66:1–66:11, 2015.
- Computer Graphics Laboratory Stanford. The Stanford 3D Scanning Repository, 2014. URL <http://graphics.stanford.edu/data/3Dscanrep/>.
- Robert E. Tarjan. Dynamic trees as search trees via euler tours, applied to the network simplex algorithm. *Mathematical Programming*, 78(2):169–177, 1997.
- Evgeny Tenetov, Gershon Wolansky, and Ron Kimmel. Fast Entropic Regularized Optimal Transport Using Semidiscrete Cost Approximation. *SIAM J. Sci. Comput.*, 40(5):A3400–A3422, 2018.

Ashish Vaswani, Noam Shazeer, Niki Parmar, Jakob Uszkoreit, Llion Jones, Aidan N. Gomez, Lukasz Kaiser, and Illia Polosukhin. Attention is All you Need. In *NeurIPS*, 2017.

Titouan Vayer, Nicolas Courty, Romain Tavenard, Laetitia Chapel, and Rémi Flamary. Optimal Transport for structured data with application on graphs. In *ICML*, 2019.

Jingdong Wang, Heng Tao Shen, Jingkuan Song, and Jianqiu Ji. Hashing for Similarity Search: A Survey. *arXiv*, 1408.2927, 2014.

Runzhong Wang, Junchi Yan, and Xiaokang Yang. Learning Combinatorial Embedding Networks for Deep Graph Matching. In *ICCV*, 2019.

Christopher K. I. Williams and Matthias Seeger. Using the Nyström Method to Speed Up Kernel Machines. In *NeurIPS*, 2001.

Bing Xiao, Xinbo Gao, Dacheng Tao, and Xuelong Li. HMM-based graph edit distance for image indexing. *Int. J. Imaging Systems and Technology*, 18(2-3):209–218, 2008.

Vinícius Flores Zambaldi, David Raposo, Adam Santoro, Victor Bapst, Yujia Li, Igor Babuschkin, Karl Tuyls, David P. Reichert, Timothy P. Lillicrap, Edward Lockhart, Murray Shanahan, Victoria Langston, Razvan Pascanu, Matthew Botvinick, Oriol Vinyals, and Peter W. Battaglia. Deep reinforcement learning with relational inductive biases. In *ICLR*, 2019.

Kai Zhang, Ivor W. Tsang, and James T. Kwok. Improved Nyström low-rank approximation and error analysis. In *ICML*, 2008.

A. Complexity analysis

Sparse Sinkhorn. A common way of achieving a high p_1 and low p_2 in LSH is via the AND-OR construction. In this scheme we calculate $B \cdot r$ hash functions, divided into B sets (hash bands) of r hash functions each. A pair of points is considered as neighbors if any hash band matches completely. Calculating the hash buckets for all points with b hash buckets per function scales as $\mathcal{O}((n+m)dBbr)$ for the hash functions we consider. As expected, for the tasks and hash functions we investigated we obtain approximately m/b^r and n/b^r neighbors, with b^r hash buckets per band. Using this we can fix the number of neighbors to a small, constant β in expectation with $b^r = \min(n, m)/\beta$. We thus obtain a sparse cost matrix \mathbf{C}^{sp} with $\mathcal{O}(\max(n, m)\beta)$ non-infinite values and can calculate \mathbf{s} and \mathbf{t} in linear time $\mathcal{O}(N_{\text{sink}} \max(n, m)\beta)$, where $N_{\text{sink}} \leq 2 + \frac{-4 \ln(\min_{i,j} \{\tilde{\mathbf{K}}_{ij} | \tilde{\mathbf{K}}_{ij} > 0\} \min_{i,j} \{\mathbf{p}_i, \mathbf{q}_j\})}{\epsilon}$ (see Theorem 4) denotes the number of Sinkhorn iterations. Calculating the hash buckets with $r = \frac{\log \min(n, m) - \log \beta}{\log b}$ takes $\mathcal{O}((n+m)dBb(\log \min(n, m) - \log \beta)/\log b)$. Since B , b , and β are small, we obtain roughly log-linear scaling with the number of points overall, i.e. $\mathcal{O}(n \log n)$ for $n \approx m$.

LCN-Sinkhorn. Both choosing landmarks via k -means++ sampling and via k -means with a fixed number of iterations have the same runtime complexity of $\mathcal{O}((n+m)ld)$. Precomputing \mathbf{W} can be done in time $\mathcal{O}(nl^2 + l^3)$. The low-rank part of updating the vectors \mathbf{s} and \mathbf{t} can be computed in $\mathcal{O}(nl + l^2 + lm)$, with l chosen constant, i.e. independently of n and m . Since sparse Sinkhorn with LSH has a log-linear runtime we again obtain log-linear overall runtime for LCN-Sinkhorn.

B. Limitations

Sparse Sinkhorn. Using a sparse approximation for \mathbf{K} works well in the common case when the regularization parameter λ is low and the cost function varies enough between data pairs, such that the transport plan \mathbf{P} resembles a sparse matrix. However, it can fail if the cost between pairs is very similar or the regularization is very high, if the dataset contains many hubs, i.e. points with a large number of neighbors, or if the distributions \mathbf{p} or \mathbf{q} are spread very unevenly. Furthermore, sparse Sinkhorn can be too unstable to train a model from scratch, since randomly initialized embeddings often have no close neighbors (see Sec. 8). Note also that LSH requires the cost function to be associated with a metric space, while regular Sinkhorn can be used with arbitrary costs.

Note that we are only interested in an approximate solution with finite error ϵ . We therefore do not need the kernel matrix to be fully indecomposable or have total support, which would be necessary and sufficient for a unique (up to

a scalar factor) and exact solution, respectively (Sinkhorn & Knopp, 1967). However, the sparse approximation is not guaranteed to have support (Def. 1), which is necessary and sufficient for the Sinkhorn algorithm to converge. The approximated matrix is actually very likely not to have support if we use one LSH bucket per sample. This is due to the non-quadratic block structure resulting from every point only having non-zero entries for points in the other data set that fall in the same bucket. We can alleviate this problem by using unbalanced OT, as proposed in Sec. 6, or (empirically) the AND-OR construction. We can also simply choose to ignore this as long as we limit the maximum number of Sinkhorn iterations. On the 3D point cloud and random data experiments we indeed ignored this issue and actually observed good performance. Experiments with other LSH schemes and the AND-OR construction showed no performance improvement despite the associated cost matrices having support. Not having support therefore seems not to be an issue in practice, at least for the data we investigated.

LCN-Sinkhorn. The LCN approximation is guaranteed to have support due to the Nyström part. Other weak spots of sparse Sinkhorn, such as very similar cost between pairs, high regularization, or data containing many hubs, are also usually handled well by the Nyström part of LCN. Highly concentrated distributions \mathbf{p} and \mathbf{q} can still have adverse effects on LCN-Sinkhorn. We can compensate for these by sampling landmarks or neighbors proportional to each point’s probability mass.

The Nyström part of LCN also has its limits, though. If the regularization parameter is low or the cost function varies greatly, we observed stability issues (over- and underflows) of the Nyström approximation because of the inverse \mathbf{A}^{-1} , which cannot be calculated in log-space. The Nyström approximation furthermore is not guaranteed to be non-negative, which can lead to catastrophic failures if the matrix product in Eq. (2) becomes negative. In these extreme cases we also observed catastrophic elimination with the correction $\mathbf{K}_{\Delta}^{\text{sp}}$. Since a low entropy regularization essentially means that optimal transport is very local, we recommend using sparse Sinkhorn in these scenarios. This again demonstrates the complementarity of the sparse approximation and Nyström: In cases where one fails we can often resort to the other.

C. Proof of Theorem 1

By linearity of expectation we obtain

$$\begin{aligned} \mathbb{E}[\mathbf{K}_{i, i_k} - \mathbf{K}_{\text{Nys}, i, i_k}] &= \mathbb{E}[\mathbf{K}_{i, i_k}] - \mathbb{E}[\mathbf{K}_{\text{Nys}, i, i_k}] \\ &= \mathbb{E}[e^{-\delta_k/\lambda}] - \mathbb{E}[\mathbf{K}_{\text{Nys}, i, i_k}] \end{aligned} \quad (20)$$

with the distance to the k th-nearest neighbor δ_k . Note that without loss of generality we can assume unit manifold

volume and obtain the integral resulting from the first expectation as (ignoring boundary effects that are exponentially small in n , see Percus & Martin (1998))

$$\mathbb{E}[e^{-\delta_k/\lambda}] \approx \frac{n!}{(n-k)!(k-1)!} \int_0^{((d/2))^{1/d}} e^{-r/\lambda} V_d(r)^{k-1} (1 - V_d(r))^{n-k} \frac{\partial V_d(r)}{\partial r} dr, \quad (21)$$

with the volume of the d -ball

$$V_d(r) = \frac{\pi^{d/2} r^d}{(d/2)!}. \quad (22)$$

Since this integral does not have an analytical solution we can either calculate it numerically or lower bound it using Jensen's inequality (again ignoring exponentially small boundary effects)

$$\mathbb{E}[e^{-\delta_k/\lambda}] \geq e^{-\mathbb{E}[\delta_k]/\lambda} \approx \exp\left(-\frac{((d/2))^{1/d} (k-1+1/d)!}{\sqrt{\pi}\lambda} \frac{n!}{(n+1/d)!}\right). \quad (23)$$

To upper bound the second expectation $\mathbb{E}[\mathbf{K}_{\text{Nys},i,i_k}]$ we now denote the distance between two points by $r_{ia} = \|\mathbf{x}_{pi} - \mathbf{x}_a\|_2$, the kernel by $k_{ia} = e^{-r_{ia}/\lambda}$ and the inter-landmark kernel matrix by \mathbf{K}_L . We first consider

$$\begin{aligned} p(\mathbf{x}_j \mid \mathbf{x}_j \text{ is } k\text{th-nearest neighbor}) &= \\ &= \int p(\delta_k = r_{ij} \mid \mathbf{x}_i, \mathbf{x}_j) p(\mathbf{x}_i) p(\mathbf{x}_j) d\mathbf{x}_i \\ &= \int p(\delta_k = r_{ij} \mid r_{ij}) p(r_{ij} \mid \mathbf{x}_j) dr_{ij} p(\mathbf{x}_j) \\ &= \int p(\delta_k = r_{ij} \mid r_{ij}) p(r_{ij}) dr_{ij} p(\mathbf{x}_j) \\ &= \int p(\delta_k = r_{ij}) dr_{ij} p(\mathbf{x}_j) \\ &= p(\mathbf{x}_j) = p(\mathbf{x}_i), \end{aligned} \quad (24)$$

where the third step is due to the uniform distribution. Since landmarks are more than $2R$ apart we can approximate

$$\mathbf{K}_L^{-1} = (\mathbf{I}_l + \mathbf{1}_{l \times l} \mathcal{O}(e^{-2R/\lambda}))^{-1} = \mathbf{I}_l - \mathbf{1}_{l \times l} \mathcal{O}(e^{-2R/\lambda}), \quad (25)$$

where $\mathbf{1}_{l \times l}$ denotes the constant 1 matrix, with the number of landmarks l . We can now use (1) the fact that landmarks are arranged apriori, (2) Hölder's inequality, (3) Eq. (24),

and (4) Eq. (25) to obtain

$$\begin{aligned} \mathbb{E}[\mathbf{K}_{\text{Nys},i,i_k}] &= \mathbb{E}\left[\sum_{a=1}^l \sum_{b=1}^l k_{ia} (\mathbf{K}_L^{-1})_{ab} k_{i_k b}\right] \\ &\stackrel{(1)}{=} \sum_{a=1}^l \sum_{b=1}^l (\mathbf{K}_L^{-1})_{ab} \mathbb{E}[k_{ia} k_{i_k b}] \\ &\stackrel{(2)}{\leq} \sum_{a=1}^l \sum_{b=1}^l (\mathbf{K}_L^{-1})_{ab} \mathbb{E}[k_{ia}^2]^{1/2} \mathbb{E}[k_{i_k b}^2]^{1/2} \\ &\stackrel{(3)}{=} \sum_{a=1}^l \sum_{b=1}^l (\mathbf{K}_L^{-1})_{ab} \mathbb{E}[k_{ia}^2]^{1/2} \mathbb{E}[k_{i_k b}^2]^{1/2} \\ &\stackrel{(4)}{=} \sum_{a=1}^l \mathbb{E}[k_{ia}^2] - \mathcal{O}(e^{-2R/\lambda}). \end{aligned} \quad (26)$$

Since landmarks are more than $2R$ apart we have $V_M \geq lV_d(R)$, where V_M denotes the volume of the manifold. Assuming Euclideaness in $V_d(R)$ we can thus use the fact that data points are uniformly distributed to obtain

$$\begin{aligned} \mathbb{E}[k_{ia}^2] &= \mathbb{E}[e^{-2r_{ia}/\lambda}] \\ &= \frac{1}{V_M} \int e^{-2r/\lambda} \frac{\partial V_d(r)}{\partial r} dr \\ &\leq \frac{1}{lV_d(R)} \int e^{-2r/\lambda} \frac{\partial V_d(r)}{\partial r} dr \\ &= \frac{1}{lV_d(R)} \int_0^R e^{-2r/\lambda} \frac{\partial V_d(r)}{\partial r} dr + \mathcal{O}(e^{-2R/\lambda}) \\ &= \frac{d}{lR^d} \int_0^R e^{-2r/\lambda} r^{d-1} dr + \mathcal{O}(e^{-2R/\lambda}) \\ &= \frac{d(\Gamma(d) - \Gamma(d, 2R/\lambda))}{l(2R/\lambda)^d} + \mathcal{O}(e^{-2R/\lambda}) \end{aligned} \quad (27)$$

and finally

$$\begin{aligned} \mathbb{E}[\mathbf{K}_{\text{Nys},i,i_k}] &\leq \sum_{a=1}^l \mathbb{E}[k_{ia}^2] - \mathcal{O}(e^{-2R/\lambda}) \\ &\leq \frac{d(\Gamma(d) - \Gamma(d, 2R/\lambda))}{(2R/\lambda)^d} + \mathcal{O}(e^{-2R/\lambda}). \end{aligned} \quad (28)$$

□

D. Proof of Theorem 2

We first prove two lemmas that will be useful later on.

Lemma A. *Let $\tilde{\mathbf{K}}$ be the Nyström approximation of the similarity matrix $\mathbf{K}_{ij} = e^{-\|\mathbf{x}_i - \mathbf{x}_j\|_2/\lambda}$, with all Nyström landmarks being at least D apart and data samples being*

no more than r away from its closest landmark. Then

$$\tilde{K}_{ij} = \tilde{K}_{ij}^{2L} + \mathcal{O}(e^{-2 \max(D-r, D/2)/\lambda}), \quad (29)$$

where \tilde{K}^{2L} denotes the Nyström approximation using only the two landmarks closest to the points \mathbf{x}_i and \mathbf{x}_j .

Proof. We denote the landmarks closest to the two points i and j with the indices a and b , or jointly with \mathbb{A} , and all other landmarks with \mathbb{C} . We furthermore denote the kernel between the point i and the point a as $k_{ia} = e^{-\|\mathbf{x}_i - \mathbf{x}_a\|_2/\lambda}$ and the vector of kernels between a set of points \mathbb{A} and a point i as $\mathbf{k}_{\mathbb{A}i}$.

We can split up A^{-1} used in the Nyström approximation

$$\tilde{K} = U A^{-1} V, \quad (30)$$

where $A_{cd} = k_{cd}$, $U_{ic} = k_{ic}$, and $V_{dj} = k_{dj}$, into relevant blocks via

$$\begin{aligned} A^{-1} &= \begin{pmatrix} A_{2L} & B \\ B^T & A_{\text{other}} \end{pmatrix}^{-1} \\ &= \begin{pmatrix} A_{2L}^{-1} + A_{2L}^{-1} B (A/A_{2L})^{-1} B^T A_{2L}^{-1} & -A_{2L}^{-1} B (A/A_{2L})^{-1} \\ -(A/A_{2L})^{-1} B^T A_{2L}^{-1} & (A/A_{2L})^{-1} \end{pmatrix}, \end{aligned} \quad (31)$$

where $A/A_{2L} = A_{\text{other}} - B^T A_{2L}^{-1} B$ denotes the Schur complement. We can thus write the entries of the Nyström approximation as

$$\begin{aligned} \tilde{K}_{ij} &= \mathbf{k}_{\mathbb{A}i}^T A_{2L}^{-1} \mathbf{k}_{\mathbb{A}j} \\ &\quad + \mathbf{k}_{\mathbb{A}i}^T A_{2L}^{-1} B (A/A_{2L})^{-1} B^T A_{2L}^{-1} \mathbf{k}_{\mathbb{A}j} \\ &\quad - \mathbf{k}_{\mathbb{A}i}^T A_{2L}^{-1} B (A/A_{2L})^{-1} \mathbf{k}_{\mathbb{C}j} \\ &\quad - \mathbf{k}_{\mathbb{C}i}^T (A/A_{2L})^{-1} B^T A_{2L}^{-1} \mathbf{k}_{\mathbb{A}j} \\ &\quad + \mathbf{k}_{\mathbb{C}i}^T (A/A_{2L})^{-1} \mathbf{k}_{\mathbb{C}j} \\ &= \tilde{K}_{ij}^{2L} + (\mathbf{k}_{\mathbb{C}i}^T - \mathbf{k}_{\mathbb{A}i}^T A_{2L}^{-1} B) \\ &\quad (A_{\text{other}} - B^T A_{2L}^{-1} B)^{-1} \\ &\quad (\mathbf{k}_{\mathbb{C}j} - B^T A_{2L}^{-1} \mathbf{k}_{\mathbb{A}j}). \end{aligned} \quad (32)$$

Interestingly, the difference to \tilde{K}_{ij}^{2L} is again a Nyström approximation where each factor is the difference between the correct kernel (e.g. $\mathbf{k}_{\mathbb{C}j}$) and the previous Nyström approximation of this kernel (e.g. $B^T A_{2L}^{-1} \mathbf{k}_{\mathbb{A}j}$).

We next bound the inverse, starting with

$$\begin{aligned} B^T A_{2L}^{-1} B &= (\mathbf{k}_{\mathbb{C}a} \quad \mathbf{k}_{\mathbb{C}b}) \frac{1}{1 - k_{ab}^2} \begin{pmatrix} 1 & -k_{ab} \\ -k_{ab} & 1 \end{pmatrix} \begin{pmatrix} \mathbf{k}_{\mathbb{C}a}^T \\ \mathbf{k}_{\mathbb{C}b}^T \end{pmatrix} \\ &= \frac{1}{1 - k_{ab}^2} (\mathbf{k}_{\mathbb{C}a} \mathbf{k}_{\mathbb{C}a}^T - k_{ab} \mathbf{k}_{\mathbb{C}a} \mathbf{k}_{\mathbb{C}b}^T - k_{ab} \mathbf{k}_{\mathbb{C}b} \mathbf{k}_{\mathbb{C}a}^T + \mathbf{k}_{\mathbb{C}b} \mathbf{k}_{\mathbb{C}b}^T) \\ &= \mathbf{1}_{l-2 \times l-2} (1 + \mathcal{O}(e^{-2D/\lambda})) \cdot 4\mathcal{O}(e^{-2D/\lambda}) \\ &= \mathbf{1}_{l-2 \times l-2} \mathcal{O}(e^{-2D/\lambda}), \end{aligned} \quad (33)$$

where $\mathbf{1}_{l-2 \times l-2}$ denotes the constant 1 matrix, with the number of landmarks l . The last steps use the fact that landmarks are more than D apart and $0 \leq k \leq 1$ for all k . For this reason we also have $A_{\text{other}} = I_{l-2} + \mathbf{1}_{l-2 \times l-2} \mathcal{O}(e^{-D/\lambda})$ and can thus use the Neumann series to obtain

$$\begin{aligned} (A_{\text{other}} - B^T A_{2L}^{-1} B)^{-1} &= (I_{l-2} + \mathbf{1}_{l-2 \times l-2} \mathcal{O}(e^{-D/\lambda}))^{-1} \\ &= I_{l-2} - \mathbf{1}_{l-2 \times l-2} \mathcal{O}(e^{-D/\lambda}). \end{aligned} \quad (34)$$

We can analogously bound the other terms in Eq. (32) to obtain

$$\begin{aligned} \tilde{K}_{ij} &= \tilde{K}_{ij}^{2L} + (\mathbf{k}_{\mathbb{C}i}^T - \mathbf{1}_{1 \times l-2} \mathcal{O}(e^{-D/\lambda})) \\ &\quad (I_{l-2} - \mathbf{1}_{l-2 \times l-2} \mathcal{O}(e^{-D/\lambda})) \\ &\quad (\mathbf{k}_{\mathbb{C}j} - \mathbf{1}_{l-2 \times 1} \mathcal{O}(e^{-D/\lambda})) \\ &\stackrel{(1)}{=} \tilde{K}_{ij}^{2L} + \mathbf{k}_{\mathbb{C}i}^T \mathbf{k}_{\mathbb{C}j} + \mathcal{O}(e^{-(D+\max(D-r, D/2))/\lambda}) \\ &= \tilde{K}_{ij}^{2L} + \sum_{\substack{1 \leq k \leq l \\ k \neq a, b}} e^{-(\|\mathbf{x}_i - \mathbf{x}_k\|_2 + \|\mathbf{x}_k - \mathbf{x}_j\|_2)/\lambda} \\ &\quad + \mathcal{O}(e^{-(D+\max(D-r, D/2))/\lambda}) \\ &\stackrel{(2)}{\leq} \tilde{K}_{ij}^{2L} + d e^{-2 \max(D-r, D/2)/\lambda} \\ &\quad + \mathcal{O}(e^{-\max(2(D-r), (1+\sqrt{3})D/2)/\lambda}) \\ &= \tilde{K}_{ij}^{2L} + \mathcal{O}(e^{-2 \max(D-r, D/2)/\lambda}), \end{aligned} \quad (35)$$

where d denotes the dimension of \mathbf{x} . Step (1) follows from the fact that any points' second closest landmarks must be at least $\max(D-r, D/2)$ away (since landmarks are at least D apart). This furthermore means that any point can have at most d second closest landmarks at this distance, which we used in step (2). \square

Lemma B. Let \tilde{K} be the Nyström approximation of the similarity matrix $K_{ij} = e^{-\|\mathbf{x}_i - \mathbf{x}_j\|_2/\lambda}$. Let \mathbf{x}_i and \mathbf{x}_j be data points with equal L_2 distance r_i and r_j to all l landmarks, which have the same distance $\Delta > 0$ to each other. Then

$$\tilde{K}_{ij} = \frac{l e^{-(r_i+r_j)/\lambda}}{1 + (l-1)e^{-\Delta/\lambda}} \quad (36)$$

Proof. The inter-landmark distance matrix is

$$A = e^{-\Delta/\lambda} \mathbf{1}_{l \times l} + (1 - e^{-\Delta/\lambda}) I_l, \quad (37)$$

where $\mathbf{1}_{l \times l}$ denotes the constant 1 matrix. Using the identity

$$(b \mathbf{1}_{n \times n} + (a-b) I_n)^{-1} = \frac{-b}{(a-b)(a+(n-1)b)} \mathbf{1}_{n \times n} + \frac{1}{a-b} I_n \quad (38)$$

we can compute

$$\begin{aligned}
 K_{ij} &= U_{i,:} A^{-1} V_{:,j} \\
 &= \begin{pmatrix} e^{-r_i/\lambda} & e^{-r_i/\lambda} & \dots \end{pmatrix} \begin{pmatrix} -e^{-\Delta/\lambda} \\ (1 - e^{-\Delta/\lambda})(1 + (l-1)e^{-\Delta/\lambda}) \mathbf{1}_{l \times l} + \frac{1}{1 - e^{-\Delta/\lambda}} \mathbf{I}_l \end{pmatrix} \begin{pmatrix} e^{-r_j/\lambda} \\ e^{-r_j/\lambda} \\ \vdots \end{pmatrix} \\
 &= \frac{e^{-(r_i+r_j)/\lambda}}{1 - e^{-\Delta/\lambda}} \left(\frac{-l^2 e^{-\Delta/\lambda}}{1 + (l-1)e^{-\Delta/\lambda}} + l \right) = \frac{e^{-(r_i+r_j)/\lambda}}{1 - e^{-\Delta/\lambda}} \frac{l - l e^{-\Delta/\lambda}}{1 + (l-1)e^{-\Delta/\lambda}} \\
 &= \frac{l e^{-(r_i+r_j)/\lambda}}{1 + (l-1)e^{-\Delta/\lambda}}.
 \end{aligned} \tag{39}$$

□

Moving on to the theorem, first note that it analyzes the maximum error realizable under the given constraints, not an expected error. K^{sp} is correct for all pairs inside a cluster and 0 otherwise. We therefore obtain the maximum error by considering the closest possible pair between clusters. By definition, this pair has distance $D - 2r$ and thus

$$\max_{\mathbf{x}_{pi}, \mathbf{x}_{qj}} K - K^{\text{sp}} = e^{-(D-2r)/\lambda} \tag{40}$$

LCN is also correct for all pairs inside a cluster, so we again consider the closest possible pair $\mathbf{x}_i, \mathbf{x}_j$ between clusters. We furthermore use Lemma A to only consider the landmarks of the two concerned clusters, adding an error of $\mathcal{O}(e^{-2(D-r)/\lambda})$, since $r \ll D$. Hence,

$$\begin{aligned}
 K_{\text{LCN},ij}^{2L} &= \begin{pmatrix} e^{-r/\lambda} & e^{-(D-r)/\lambda} \end{pmatrix} \begin{pmatrix} 1 & e^{-D/\lambda} \\ e^{-D/\lambda} & 1 \end{pmatrix}^{-1} \begin{pmatrix} e^{-(D-r)/\lambda} \\ e^{-r/\lambda} \end{pmatrix} \\
 &= \frac{1}{1 - e^{-2D/\lambda}} \begin{pmatrix} e^{-r/\lambda} & e^{-(D-r)/\lambda} \end{pmatrix} \begin{pmatrix} 1 & e^{-D/\lambda} \\ -e^{-D/\lambda} & 1 \end{pmatrix} \begin{pmatrix} e^{-(D-r)/\lambda} \\ e^{-r/\lambda} \end{pmatrix} \\
 &= \frac{1}{1 - e^{-2D/\lambda}} \begin{pmatrix} e^{-r/\lambda} & e^{-(D-r)/\lambda} \end{pmatrix} \begin{pmatrix} e^{-(D-r)/\lambda} - e^{-(D+r)/\lambda} \\ e^{-r/\lambda} - e^{-(2D-r)/\lambda} \end{pmatrix} \\
 &= \frac{1}{1 - e^{-2D/\lambda}} (e^{-D/\lambda} - e^{-(D+2r)/\lambda} + e^{-D/\lambda} - e^{-(3D-2r)/\lambda}) \\
 &= \frac{e^{-D/\lambda}}{1 - e^{-2D/\lambda}} (2 - e^{-2r/\lambda} - e^{-(2D-2r)/\lambda}) \\
 &= e^{-D/\lambda} (2 - e^{-2r/\lambda}) - \mathcal{O}(e^{-2(D-r)/\lambda})
 \end{aligned} \tag{41}$$

and thus

$$\begin{aligned}
 \max_{\mathbf{x}_{pi}, \mathbf{x}_{qj}} K - K_{\text{LCN}} &= e^{-(D-2r)/\lambda} (1 - e^{-2r/\lambda} (2 - e^{-2r/\lambda})) \\
 &\quad + \mathcal{O}(e^{-2D/\lambda}).
 \end{aligned} \tag{42}$$

For pure Nyström we need to consider the distances inside a cluster. In the worst case two points overlap, i.e. $K_{ij} = 1$, and lie at the boundary of the cluster. Since $r \ll D$ we again use Lemma A to only consider the landmark in the concerned cluster, adding an error of $\mathcal{O}(e^{-2(D-r)/\lambda})$.

$$K_{\text{Nys},ij} = e^{-2r/\lambda} + \mathcal{O}(e^{-2(D-r)/\lambda}) \tag{43}$$

□

Note that when ignoring the effect from other clusters we can generalize the Nyström error to $l \leq d$ landmarks per

cluster. In this case, because of symmetry we can optimize the worst-case distance from all cluster landmarks by putting them on an $(l-1)$ -simplex centered on the cluster center. Since there are at most d landmarks in each cluster there is always one direction in which the worst-case points are r away from all landmarks. The circumradius of an $(l-1)$ -simplex with side length Δ is $\sqrt{\frac{l-1}{2l}} \Delta$. Thus, the maximum distance to all landmarks is $\sqrt{r^2 + \frac{l-1}{2l} \Delta^2}$. Using Lemma B we therefore obtain the Nyström approximation

$$K_{\text{Nys},ij}^{\text{multi}} = \frac{l e^{-2\sqrt{r^2 + \frac{l-1}{2l} \Delta^2}/\lambda}}{1 + (l-1)e^{-\Delta/\lambda}} + \mathcal{O}(e^{-2(D-r)/\lambda}) \tag{44}$$

E. Notes on Theorem 3

Lemmas C-F and thus Theorem 1 by Altschuler et al. (2019) are also valid for \mathbf{Q} outside the simplex so long as $\|\mathbf{Q}\|_1 = \sum_{i,j} |\mathbf{Q}_{ij}| = n$ and it only has non-negative entries. Any $\hat{\mathbf{P}}$ returned by Sinkhorn fulfills these conditions if the kernel matrix is non-negative and has support. Therefore the rounding procedure given by their Algorithm 4 is not necessary for this result.

Furthermore, to be more consistent with Theorems 1 and 2 we use the L_2 distance instead of L_2^2 in this theorem, which only changes the dependence on ρ .

F. Notes on Theorem 4

To adapt Theorem 1 by Dvurechensky et al. (2018) to sparse matrices (i.e. matrices with some $K_{ij} = 0$) we need to redefine

$$\nu := \min_{i,j} \{K_{ij} | K_{ij} > 0\}, \tag{45}$$

i.e. take the minimum only w.r.t. non-zero elements in their Lemma 1. We furthermore need to consider sums exclusively over these non-zero elements instead of the full $\mathbf{1}$ vector in their Lemma 1.

The Sinkhorn algorithm converges since the matrix has support (Sinkhorn & Knopp, 1967). However, the point it converges to might not exist because we only require support, not total support. Therefore, we need to consider slightly perturbed optimal vectors for the proof, i.e. define a negligibly small $\tilde{\varepsilon} \ll \varepsilon, \varepsilon'$ for which $|B(u^*, v^*) \mathbf{1} - r| \leq \tilde{\varepsilon}$, $|B(u^*, v^*)^T \mathbf{1} - c| \leq \tilde{\varepsilon}$. Support furthermore guarantees that no row or column is completely zero, thus preventing any unconstrained u_k or v_k , and any non-converging row or column sum of $B(u_k, v_k)$. With these changes in place all proofs work the same as in the dense case.

G. Proof of Proposition 1

Theorem A (Danskin’s theorem). *Consider a continuous function $\phi : \mathbb{R}^k \times Z \rightarrow \mathbb{R}$, with the compact set $Z \subset \mathbb{R}^j$. If $\phi(\mathbf{x}, \mathbf{z})$ is convex in \mathbf{x} for every $\mathbf{z} \in Z$ and $\phi(\mathbf{x}, \mathbf{z})$ has a unique maximizer $\bar{\mathbf{z}}$, the derivative of*

$$f(\mathbf{x}) = \max_{\mathbf{z} \in Z} \phi(\mathbf{x}, \mathbf{z}) \quad (46)$$

is given by the derivative at the maximizer, i.e.

$$\frac{\partial f}{\partial \mathbf{x}} = \frac{\partial \phi(\mathbf{x}, \bar{\mathbf{z}})}{\partial \mathbf{x}}. \quad (47)$$

We start by deriving the derivatives of the distances. To show that the Sinkhorn distance fulfills the conditions for Danskin’s theorem we first identify $\mathbf{x} = \mathbf{C}$, $\mathbf{z} = \mathbf{P}$, and $\phi(\mathbf{C}, \mathbf{P}) = -\langle \mathbf{P}, \mathbf{C} \rangle_F + \lambda H(\mathbf{P})$. We next observe that the restrictions $\mathbf{P}\mathbf{1}_m = \mathbf{p}$ and $\mathbf{P}^T\mathbf{1}_n = \mathbf{q}$ define a compact, convex set for \mathbf{P} . Furthermore, ϕ is a continuous function and linear in \mathbf{C} , i.e. both convex and concave for any finite \mathbf{P} . Finally, $\phi(\mathbf{C}, \mathbf{P})$ is concave in \mathbf{P} since $\langle \mathbf{P}, \mathbf{C} \rangle_F$ is linear and $\lambda H(\mathbf{P})$ is concave. Therefore the maximizer $\bar{\mathbf{P}}$ is unique and Danskin’s theorem applies to the Sinkhorn distance. Using

$$\begin{aligned} \frac{\partial C_{Nys,ij}}{\partial U_{kl}} &= \frac{\partial}{\partial U_{kl}} \left(-\lambda \log \left(\sum_a U_{ia} W_{aj} \right) \right) \\ &= -\lambda \delta_{ik} \frac{W_{lj}}{\sum_a U_{ia} W_{aj}} = -\lambda \delta_{ik} \frac{W_{lj}}{K_{Nys,ij}}, \end{aligned} \quad (48)$$

$$\begin{aligned} \frac{\partial C_{Nys,ij}}{\partial W_{kl}} &= \frac{\partial}{\partial W_{kl}} \left(-\lambda \log \left(\sum_a U_{ia} W_{aj} \right) \right) \\ &= -\lambda \delta_{jl} \frac{U_{ik}}{\sum_a U_{ia} W_{aj}} = -\lambda \delta_{jl} \frac{U_{ik}}{K_{Nys,ij}}, \end{aligned} \quad (49)$$

$$\begin{aligned} \frac{\bar{P}_{Nys,ij}}{K_{Nys,ij}} &= \frac{\sum_b \bar{P}_{U,ib} \bar{P}_{W,bj}}{\sum_a U_{ia} W_{aj}} = \frac{\bar{s}_i \bar{t}_j \sum_b U_{ib} W_{bj}}{\sum_a U_{ia} W_{aj}} \\ &= \bar{s}_i \bar{t}_j \frac{\sum_b U_{ib} W_{bj}}{\sum_a U_{ia} W_{aj}} = \bar{s}_i \bar{t}_j \end{aligned} \quad (50)$$

and the chain rule we can calculate the derivative w.r.t. the cost matrix as

$$\frac{\partial d_c^\lambda}{\partial \mathbf{C}} = -\frac{\partial}{\partial \mathbf{C}} (-\langle \bar{\mathbf{P}}, \mathbf{C} \rangle_F + \lambda H(\bar{\mathbf{P}})) = \bar{\mathbf{P}}, \quad (51)$$

$$\begin{aligned} \frac{\partial d_{LCN,c}^\lambda}{\partial U_{kl}} &= \sum_{i,j} \frac{\partial C_{Nys,ij}}{\partial U_{kl}} \frac{\partial d_{LCN,c}^\lambda}{\partial C_{Nys,ij}} = -\lambda \sum_{i,j} \delta_{ik} W_{lj} \frac{\bar{P}_{Nys,ij}}{K_{Nys,ij}} \\ &= -\lambda \sum_{i,j} \delta_{ik} W_{lj} \bar{s}_i \bar{t}_j = -\lambda \bar{s}_k \sum_j W_{lj} \bar{t}_j \\ &= (-\lambda \bar{\mathbf{s}}(\mathbf{W}\bar{\mathbf{t}})^T)_{kl}, \end{aligned} \quad (52)$$

$$\begin{aligned} \frac{\partial d_{LCN,c}^\lambda}{\partial W_{kl}} &= \sum_{i,j} \frac{\partial C_{Nys,ij}}{\partial W_{kl}} \frac{\partial d_{LCN,c}^\lambda}{\partial C_{Nys,ij}} = -\lambda \sum_{i,j} \delta_{jl} U_{ik} \frac{\bar{P}_{Nys,ij}}{K_{Nys,ij}} \\ &= -\lambda \sum_{i,j} \delta_{jl} U_{ik} \bar{s}_i \bar{t}_j = -\lambda \left(\sum_i \bar{s}_i U_{ik} \right) \bar{t}_l \\ &= (-\lambda (\bar{\mathbf{s}}^T \mathbf{U})^T \bar{\mathbf{t}}^T)_{kl}, \end{aligned} \quad (53)$$

and $\frac{\partial d_{LCN,c}^\lambda}{\partial \log K^{\text{sp}}}$ and $\frac{\partial d_{LCN,c}^\lambda}{\partial \log K_{Nys}^{\text{sp}}}$ follow directly from $\frac{\partial d_c^\lambda}{\partial \mathbf{C}}$. We can then backpropagate in time $\mathcal{O}((n+m)l^2)$ by computing the matrix-vector multiplications in the right order. \square

H. Choosing LSH neighbors and Nyström landmarks

We focus on two LSH methods for obtaining near neighbors. Cross-polytope LSH (Andoni et al., 2015) uses a random projection matrix $\mathbf{R} \in \mathbb{R}^{d \times b/2}$ with the number of hash buckets b , and then decides on the hash bucket via $h(\mathbf{x}) = \arg \max(\|\mathbf{x}^T \mathbf{R}\| - \mathbf{x}^T \mathbf{R})$, where $\|$ denotes concatenation. k -means LSH computes k -means and uses the clusters as hash buckets.

We further improve the sampling probabilities of cross-polytope LSH via the AND-OR construction. In this scheme we calculate $B \cdot r$ hash functions, divided into B sets (hash bands) of r hash functions each. A pair of points is considered as neighbors if any hash band matches completely. k -means LSH does not work well with the AND-OR construction since its samples are highly correlated. For large datasets we use hierarchical k -means instead (Paulevé et al., 2010; Nistér & Stewénus, 2006).

The 3D point clouds, uniform data and the graph transport network (GTN) use the L_2 distance between embeddings as a cost function. For these we use (hierarchical) k -means LSH and k -means Nyström in both sparse Sinkhorn and LCN-Sinkhorn.

Word embedding similarities are measured via a dot product. In this case we use cross-polytope LSH for sparse Sinkhorn in this case. For LCN-Sinkhorn we found that using k -means LSH works better with Nyström using k -means++ sampling than cross-polytope LSH. This is most likely due to a better alignment between LSH samples and Nyström. We convert the cosine similarity to a distance via $d_{\cos} = \sqrt{1 - \frac{\mathbf{x}_p^T \mathbf{x}_q}{\|\mathbf{x}_p\|_2 \|\mathbf{x}_q\|_2}}$ (Berg et al., 1984) to use k -means with dot product similarity. Note that this is actually based on cosine similarity, not the dot product. Due to the balanced nature of OT we found this more sensible than maximum inner product search (MIPS). For both experiments we also experimented with uniform and recursive RLS sampling but found that the above mentioned methods work better.

I. Implementational details

Our implementation runs in batches on a GPU via PyTorch (Paszke et al., 2019) and PyTorch Scatter (Fey & Lenssen, 2019). To avoid over- and underflows we use log-stabilization throughout, i.e. we save all values in log-space and compute all matrix-vector products and additions via the log-sum-exp trick $\log \sum_i e^{x_i} = \max_j x_j + \log(\sum_i e^{x_i - \max_j x_j})$. Since the matrix \mathbf{A} is small we compute its inverse using double precision to improve stability. Surprisingly, we did not observe any benefit from using the Cholesky decomposition or not calculating \mathbf{A}^{-1} and instead solving the equation $\mathbf{B} = \mathbf{A}\mathbf{X}$ for \mathbf{X} . We furthermore precompute $\mathbf{W} = \mathbf{A}^{-1}\mathbf{V}$ to avoid unnecessary operations.

We use 3 layers and an embedding size $H_N = 32$ for GTN. The MLPs use a single hidden layer, biases and LeakyReLU non-linearities. The single-head MLP uses an output size of $H_{N, \text{match}} = H_N$ and a hidden embedding size of $4H_N$, i.e. the same as the concatenated node embedding, and the multi-head MLP uses a hidden embedding size of H_N . To stabilize initial training we scale the node embeddings by $\frac{\bar{d}}{\bar{n}\sqrt{H_{N, \text{match}}}}$

directly before calculating OT. \bar{d} denotes the average graph distance in the training set, \bar{n} the average number of nodes per graph, and $H_{N, \text{match}}$ the matching embedding size, i.e. 32 for single-head and 128 for multi-head OT.

For the graph datasets, the 3D point clouds and random data we use the L_2 distance for the cost function. For word embedding alignment we use the dot product, since this best resembles their generation procedure.

J. Graph dataset generation and experimental details

The dataset statistics are summarized in Table 5. Each dataset contains the distances between all graph pairs in each split, i.e. 10296 and 1128 distances for preferential attachment. The AIDS dataset was generated by randomly sampling graphs with at most 30 nodes from the original AIDS dataset (Riesen & Bunke, 2008). Since not all node types are present in the training set and our choice of GED is permutation-invariant w.r.t. types, we permuted the node types so that there are no previously unseen types in the validation and test sets. For the preferential attachment datasets we first generated 12, 4, and 4 undirected “seed” graphs (for train, val, and test) via the initial attractiveness model with randomly chosen parameters: 1 to 5 initial nodes, initial attractiveness of 0 to 4 and $1/2\bar{n}$ and $3/2\bar{n}$ total nodes, where \bar{n} is the average number of nodes (20, 200, 2000, and 20000). We then randomly label every node (and edge) in these graphs uniformly. To obtain the remaining graphs we edit the “seed” graphs between $\bar{n}/40$ and $\bar{n}/20$ times by randomly adding, type editing, or removing nodes and edges.

Editing nodes and edges is 4x and adding/deleting edges 3x as likely as adding/deleting nodes. Most of these numbers were chosen arbitrarily, aiming to achieve a somewhat reasonable dataset and process. We found that the process of first generating seed graphs and subsequently editing these is crucial for obtaining meaningfully structured data to learn from. For the GED we choose an edit cost of 1 for changing a node or edge type and 2 for adding or deleting a node or an edge.

We represent node and edge types as one-hot vectors. We train all models except SiamMPNN (which uses SGD) and GTN on Linux with the Adam optimizer and mean squared error (MSE) loss for up to 300 epochs and reduce the learning rate by a factor of 10 every 100 steps. On Linux we train for up to 1000 epochs and reduce the learning rate by a factor of 2 every 100 steps. We use the parameters from the best epoch based on the validation set. We choose hyperparameters for all models using multiple steps of grid search on the validation set, see Tables 6 to 8 for the final values. We use the originally published result of SimGNN on Linux and thus don’t provide its hyperparameters. GTN uses 500 Sinkhorn iterations. We obtain the final entropy regularization parameter from λ_{base} via $\lambda = \lambda_{\text{base}} \frac{\bar{d}}{\bar{n}} \frac{1}{\log n}$, where \bar{d} denotes the average graph distance and \bar{n} the average number of nodes per graph in the training set. The factor \bar{d}/\bar{n} serves to estimate the embedding distance scale and $1/\log n$ counteracts the entropy scaling with $n \log n$. Note that the entropy regularization parameter was small, but always far from 0, which shows that entropy regularization actually has a positive effect on learning. On the pref. att. 200 dataset we use no L_2 regularization, $\lambda_{\text{base}} = 0.5$, and a batch size of 200. For pref. att. 2k we use $\lambda_{\text{base}} = 2$ and a batch size of 20 for full Sinkhorn and 100 for LCN-Sinkhorn. For pref. att. 20k we use $\lambda_{\text{base}} = 50$ and a batch size of 4. λ_{base} scales with graph size due to normalization of the PM kernel.

For LCN-Sinkhorn we use roughly 10 neighbors for LSH (20 k -means clusters) and 10 k -means landmarks for Nyström on pref. att. 200. We double these numbers for pure Nyström Sinkhorn, sparse Sinkhorn, and multiscale OT. For pref. att. 2k we use around 15 neighbors (10 · 20 hierarchical clusters) and 15 landmarks and for pref. att. 20k we use roughly 30 neighbors (10 · 10 · 10 hierarchical clusters) and 20 landmarks. The number of neighbors for the 20k dataset is higher and strongly varies per iteration due to the unbalanced nature of hierarchical k -means. This increase in neighbors and landmarks and PyTorch’s missing support for ragged tensors largely explains LCN-Sinkhorn’s deviation from perfectly linear runtime scaling.

We perform all runtime measurements on a compute node using one Nvidia GeForce GTX 1080 Ti, two Intel Xeon E5-2630 v4, and 256GB RAM.

Table 5: Graph dataset statistics.

	Graph type	Distance	Distance (test set)		Graphs train/val/test	Avg. nodes per graph	Avg. edges per graph	Node types	Edge types
			Mean	Std. dev.					
AIDS30	Molecules	GED	50.5	16.2	144/48/48	20.6	44.6	53	4
Linux	Program dependence	GED	0.567	0.181	600/200/200	7.6	6.9	7	-
Pref. att.	Initial attractiveness	GED	106.7	48.3	144/48/48	20.6	75.4	6	4
Pref. att. 200	Initial attractiveness	PM	0.400	0.102	144/48/48	199.3	938.8	6	-
Pref. att. 2k	Initial attractiveness	PM	0.359	0.163	144/48/48	2045.6	11330	6	-
Pref. att. 20k	Initial attractiveness	PM	0.363	0.151	144/48/48	20441	90412	6	-

Table 6: Hyperparameters for the Linux dataset.

	lr	batchsize	layers	emb. size	L_2 reg.	λ_{base}
SiamMPNN	1×10^{-4}	256	3	32	5×10^{-4}	-
GMN	1×10^{-4}	20	3	64	0	-
GTN, 1 head	0.01	1000	3	32	1×10^{-6}	1.0
8 OT heads	0.01	1000	3	32	1×10^{-6}	1.0
Balanced OT	0.01	1000	3	32	1×10^{-6}	2.0

Table 7: Hyperparameters for the AIDS dataset.

	lr	batchsize	layers	emb. size	L_2 reg.	λ_{base}
SiamMPNN	1×10^{-4}	256	3	32	5×10^{-4}	-
SimGNN	1×10^{-3}	1	3	32	0.01	-
GMN	1×10^{-2}	128	3	32	0	-
GTN, 1 head	0.01	100	3	32	5×10^{-3}	0.1
8 OT heads	0.01	100	3	32	5×10^{-3}	0.075
Balanced OT	0.01	100	3	32	5×10^{-3}	0.1
Nyström	0.015	100	3	32	5×10^{-3}	0.2
Multiscale	0.015	100	3	32	5×10^{-3}	0.2
Sparse OT	0.015	100	3	32	5×10^{-3}	0.2
LCN-OT	0.015	100	3	32	5×10^{-3}	0.2

Table 8: Hyperparameters for the preferential attachment GED dataset.

	lr	batchsize	layers	emb. size	L_2 reg.	λ_{base}
SiamMPNN	1×10^{-4}	256	3	64	1×10^{-3}	-
SimGNN	1×10^{-3}	4	3	32	0	-
GMN	1×10^{-4}	20	3	64	0	-
GTN, 1 head	0.01	100	3	32	5×10^{-4}	0.2
8 OT heads	0.01	100	3	32	5×10^{-3}	0.075
Balanced OT	0.01	100	3	32	5×10^{-4}	0.2
Nyström	0.02	100	3	32	5×10^{-5}	0.2
Multiscale	0.02	100	3	32	5×10^{-5}	0.2
Sparse OT	0.02	100	3	32	5×10^{-5}	0.2
LCN-OT	0.02	100	3	32	5×10^{-5}	0.2

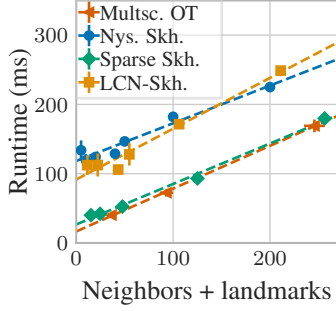


Figure 3: Runtime scales linearly with the number of neighbors/landmarks for all relevant Sinkhorn approximation methods.

K. Runtimes

Table 9 compares the runtime of the full Sinkhorn distance with different approximation methods using 40 neighbors/landmarks. We separate the computation of approximate \mathbf{K} from the optimal transport computation (Sinkhorn iterations), since the former primarily depends on the LSH and Nyström methods we choose. We observe a 2-4x speed difference between sparse (multiscale OT and sparse Sinkhorn) and low-rank approximations (Nyström Sinkhorn and LCN-Sinkhorn), while factored OT is multiple times slower due to its iterative refinement scheme. In Fig. 3 we observe that this runtime gap stays constant independent of the number of neighbors/landmarks, i.e. the relative difference decreases as we increase the number of neighbors/landmarks. This gap could either be due to details in low-level CUDA implementations and hardware or the fact that low-rank approximations require 2x as many multiplications for the same number of neighbors/landmarks. In either case, both Table 9 and Fig. 3 show that the runtimes of all approximations scale linearly both in the dataset size and the number of neighbors and landmarks, while full Sinkhorn scales quadratically.

We furthermore investigate whether GTN with approximate Sinkhorn indeed scales log-linearly with the graph size by generating preferential attachment graphs with 200, 2000, and 20 000 nodes ($\pm 50\%$). We use the Pyramid matching (PM) kernel (Nikolentzos et al., 2017) as prediction target. Fig. 4 shows that the runtime of LCN-Sinkhorn scales almost linearly (dashed line) and regular full Sinkhorn quadratically (dash-dotted line) with the number of nodes, despite both achieving similar accuracy and LCN using slightly more neighbors and landmarks on larger graphs to sustain good accuracy. Full Sinkhorn went out of memory for the largest graphs.

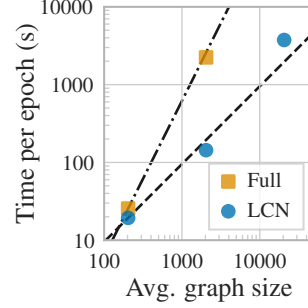


Figure 4: Log-log runtime per epoch for GTN with full Sinkhorn and LCN-Sinkhorn. LCN-Sinkhorn scales almost linearly with graph size while sustaining similar accuracy.

L. Distance approximation

Fig. 5 shows that for the chosen $\lambda = 0.05$ sparse Sinkhorn offers the best trade-off between computational budget and distance approximation, with LCN-Sinkhorn and multiscale OT coming in second. Factored OT is again multiple times slower than the other methods. Note that d_c^λ can be negative due to the entropy offset. This picture changes as we increase the regularization. For higher regularizations LCN-Sinkhorn is the most precise at constant computational budget (number of neighbors/landmarks). Note that the crossover points in this figure roughly coincide with those in Fig. 2. Keep in mind that usually the OT plan is more important than the raw distance approximation, since it determines the training gradient and tasks like embedding alignment don't use the distance at all. This becomes evident in the fact that sparse Sinkhorn achieves a better distance approximation than LCN-Sinkhorn but performs worse in both downstream tasks investigated in Sec. 8.

Table 9: Runtimes (ms) of Sinkhorn approximations for EN-DE embeddings at different dataset sizes. Full Sinkhorn scales quadratically, while all approximations scale at most linearly with the size. Sparse approximations are 2-4x faster than low-rank approximations, and factored OT is multiple times slower due to its iterative refinement scheme. Note that similarity matrix computation time (K) primarily depends on the LSH/Nyström method, not the OT approximation.

	$N = 10000$		$N = 20000$		$N = 50000$	
	K	OT	K	OT	K	OT
Full Sinkhorn	8	2950	29	11 760	OOM	OOM
Factored OT	29	809	32	1016	55	3673
Multiscale OT	90	48	193	61	521	126
Nyström Skh.	29	135	41	281	79	683
Sparse Skh.	42	46	84	68	220	137
LCN-Sinkhorn	101	116	242	205	642	624

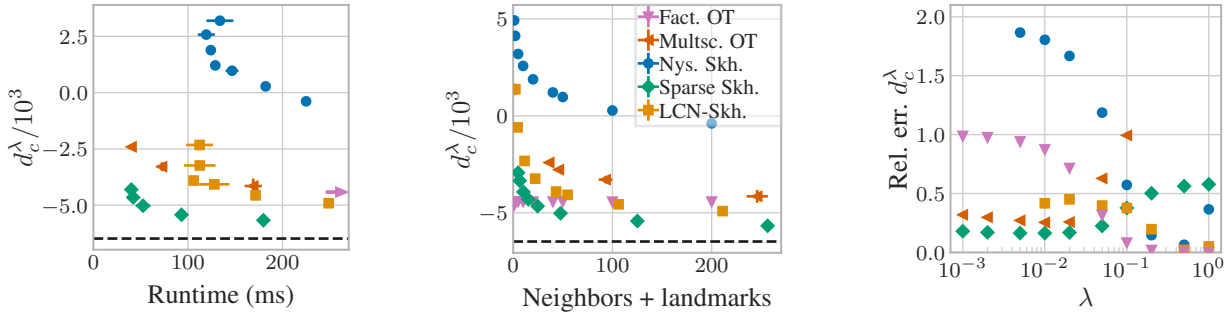


Figure 5: Sinkhorn distance approximation for different runtimes and computational budgets (both varied via the number of neighbors/landmarks), and entropy regularization parameters λ . The dashed line denotes the true Sinkhorn distance. The arrow indicates factored OT results far outside the depicted range. **Left:** Sparse Sinkhorn consistently performs best across all runtimes. **Center:** Sparse Sinkhorn mostly performs best, with LCN-Sinkhorn coming in second, and factored OT being seemingly independent from the number of neighbors. **Right:** Sparse Sinkhorn performs best for low λ , LCN-Sinkhorn for moderate and high λ and factored OT for very high λ .